Dual recognition of chromatin and microtubules by INCENP is important for mitotic progression

Michael S. Wheelock,[1] David J. Wynne,[1,2] Boo Shan Tseng,[1,3] and Hironori Funabiki[1]

[1]Laboratory of Chromosome and Cell Biology, The Rockefeller University, New York, NY 10065
[2]Department of Biology, The College of New Jersey, Ewing, NJ 08628
[3]The School of Life Sciences, The University of Nevada Las Vegas, Las Vegas, NV 89154

The chromosomal passenger complex (CPC), composed of inner centromere protein (INCENP), Survivin, Borealin, and the kinase Aurora B, contributes to the activation of the mitotic checkpoint. The regulation of CPC function remains unclear. Here, we reveal that in addition to Survivin and Borealin, the single α-helix (SAH) domain of INCENP supports CPC localization to chromatin and the mitotic checkpoint. The INCENP SAH domain also mediates INCENP's microtubule binding, which is negatively regulated by Cyclin-dependent kinase–mediated phosphorylation of segments flanking the SAH domain. The microtubule-binding capacity of the SAH domain is important for mitotic arrest in conditions of suppressed microtubule dynamics, and the duration of mitotic arrest dictates the probability, but not the timing, of cell death. Although independent targeting of INCENP to microtubules or the kinetochore/centromere promotes the mitotic checkpoint, it is insufficient for a robust mitotic arrest. Altogether, our results demonstrate that dual recognition of chromatin and microtubules by CPC is important for checkpoint maintenance and determination of cell fate in mitosis.

Introduction

Accurate chromosome segregation requires bipolar attachment of microtubules (MTs) to the kinetochore. Unattached kinetochores activate the mitotic checkpoint (or spindle assembly checkpoint [SAC]) to delay anaphase onset while erroneous kinetochore microtubule (kMT) attachments are being corrected (Foley and Kapoor, 2013). Both processes are promoted by the chromosomal passenger complex (CPC), composed of inner centromere protein (INCENP), Survivin, Borealin (also known as Dasra and CDCA8), and the kinase Aurora B (Carmena et al., 2012; Trivedi and Stukenberg, 2016).

The CPC regulates error correction and the SAC by phosphorylating multiple substrates at the kinetochore. First, Aurora B destabilizes kMT attachment by phosphorylating the MT-binding protein Hec1 (Ndc80; DeLuca et al., 2006; Welburn et al., 2010), generating unattached kinetochores that can signal the SAC (Etemad et al., 2015; Tauchman et al., 2015). Second, Aurora B promotes kinetochore recruitment of Mps1 (Saurin et al., 2011; van der Waal et al., 2012; Nijenhuis et al., 2013; Zhu et al., 2013), which stimulates the SAC by phosphorylating KNL1 (London et al., 2012; Shepperd et al., 2012; Yamagishi et al., 2012; Vleugel et al., 2015). Phosphorylated KNL1 further recruits the SAC proteins Bub1, Bub3, BubR1, Mad1, and Mad2 (Zich et al., 2012; Primorac et al., 2013; Tipton et al., 2013; London and Biggins, 2014). Third, Aurora B promotes kinetochore recruitment of KNL1 and the Ndc80 complex by phosphorylating Dsn1, a subunit of the Mis12 complex (Yang et al., 2008; Akiyoshi et al., 2013; Kim and Yu, 2015). Finally, Aurora B antagonizes protein phosphatase 1 (PP1)-mediated silencing of the SAC by phosphorylating the PP1 binding motif on KNL1 to prevent PP1 localization (Liu et al., 2010; Rosenberg et al., 2011). Aurora B–dependent phosphorylation is high on unattached or erroneously attached kinetochores but low on bioriented kinetochores that are under MT-dependent tension (Knowlton et al., 2006; Liu et al., 2009; Welburn et al., 2010; DeLuca et al., 2011). How Aurora B–dependent kinetochore phosphorylation responds to kMT attachment status remains unclear.

Aurora B activation depends on its interaction with the C-terminal IN-box motif of INCENP and on autophosphorylation of Aurora B and INCENP (Adams et al., 2000; Bishop and Schumacher, 2002; Honda et al., 2003; Sessa et al., 2005). Because this autophosphorylation is facilitated by local enrichment of the CPC (Kelly et al., 2007), Aurora B activity is often coupled to its localization. During early mitosis, the CPC is enriched at the inner centromere through Survivin and Borealin (Gassmann et al., 2004; Sampath et al., 2004), which form a trimeric complex with the N-terminal CEN domain of INC ENP (Klein et al., 2006; Jeyaprakash et al., 2007). Survivin

Correspondence to Hironori Funabiki: funabih@rockefeller.edu

Abbreviations used: CPC, chromosomal passenger complex; CSF, cytostatic factor; DoM, duration of mitosis; FL, full length; INCENP, inner centromere protein; IQR, interquartile range; kMT, kinetochore microtubule; MT, microtubule; MTBD, microtubule-binding domain; NEB, nuclear envelope breakdown; PP, protein phosphatase; PRD, phospho-regulatory domain; SAC, spindle assembly checkpoint; SAH, single α-helix.

The Rockefeller University Press $30.00
J. Cell Biol. Vol. 216 No. 4 925–941
https://doi.org/10.1083/jcb.201609061

interacts directly with histone H3 phosphorylated at threonine 3 (H3T3ph; Kelly et al., 2010; Wang et al., 2010; Yamagishi et al., 2010), whereas Borealin indirectly binds histone H2A phosphorylated at threonine 120 (H2A T120ph; Tsukahara et al., 2010). However, the roles of CPC at the centromere in kMT regulation and SAC activation have been questioned in budding yeast (Campbell and Desai, 2013).

The CPC also interacts weakly with spindle MTs during early mitosis (Tseng et al., 2010). The interaction of Aurora B and EB1 at growing MT ends stimulates recruitment of the CPC to the inner centromere by promoting feedback between Aurora B and Bub1 (Banerjee et al., 2014). Ubiquitylated Aurora B also interacts with UBASH3B/MKLP2 on MTs and is required to concentrate the CPC at the inner centromere (Krupina et al., 2016). In addition, the CPC binds MTs directly through the single α-helix (SAH) domain (previously termed the putative coiled-coil domain) of INCENP (Mackay et al., 1993; Tseng et al., 2010; Samejima et al., 2015; van der Horst et al., 2015). The SAH domain is essential for viability in chicken DT40 cells, effective Dsn1 phosphorylation, and CPC relocalization to the spindle midzone at anaphase in human cells (Samejima et al., 2015; van der Horst et al., 2015). It was also reported that deleting the SAH domain attenuates the SAC in taxol-treated human cells without affecting centromeric localization of the CPC (Vader et al., 2007). Here, we investigate the molecular mechanism by which the SAH domain regulates kinetochore phosphorylation by Aurora B and contributes to the SAC.

Results

The INCENP SAH domain is required for CPC localization to chromatin and the SAC in *Xenopus* egg extracts

The nocodazole-induced SAC depends on Aurora B in *Xenopus laevis* egg extracts (Kallio et al., 2002; Vigneron et al., 2004; Gadea and Ruderman, 2005). To determine whether the INCENP SAH domain is required for the SAC in this system, the CPC was depleted from M-phase extract and reconstituted with GFP-tagged full-length *Xenopus* INCENP (xINCENP) or xINCENP ΔSAH (Fig. 1 A). The SAC was assayed by adding a high concentration of sperm nuclei and nocodazole, followed by calcium to release the cytostatic factor (CSF)-mediated metaphase arrest (Minshull et al., 1994). Mock-depleted extract remained in M phase with high H3T3ph levels for the duration of the assay, indicative of a SAC arrest, whereas CPC-depleted extract (ΔCPC) exited into interphase within 30 min after calcium addition. This defect was fully rescued when the extract was reconstituted with CPC containing xINCENP but not xINCENP ΔSAH, indicating that the SAH domain is required for the SAC in *Xenopus* egg extract. Although xINCENP was broadly distributed along sperm chromatin with enrichment near the centromere, the level of xINCENP ΔSAH on chromatin was dramatically reduced (Fig. 1 B). A similar localization defect on preassembled CENP-A chromatin arrays in M-phase extract was also observed (Fig. 1 C).

When a GFP-tagged SAH domain fragment (xSAH) was expressed in M-phase extract, it localized weakly and broadly along sperm chromatin (Fig. 1 D). This localization was independent of endogenous INCENP, as 6Myc-tagged xSAH

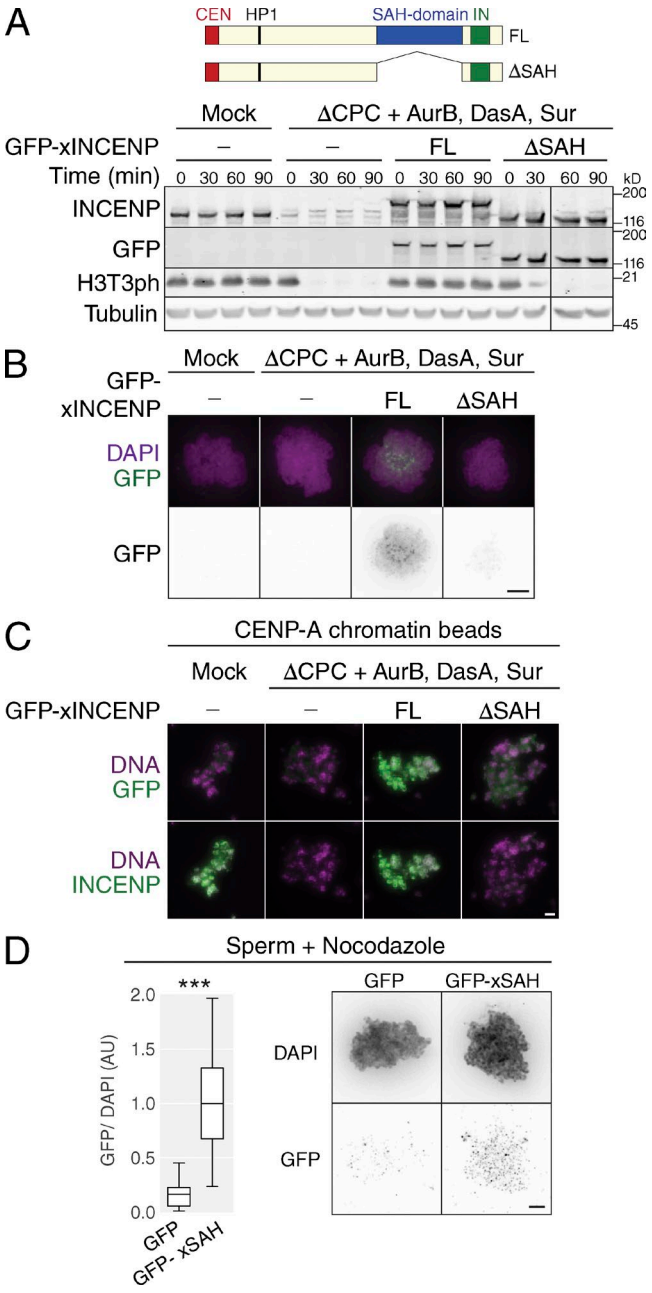

Figure 1. **The SAH domain is required for CPC localization and the SAC in *Xenopus*.** (A) Top, diagram of INCENP constructs. CEN, centromere-targeting domain; IN, IN-box; HP1, HP1-binding motif. Bottom, *Xenopus* egg extracts were either mock depleted (Mock) or depleted of CPC (ΔCPC); reconstituted with xAurora B, xDasra A, xSurvivin, and FL or ΔSAH GFP-INCENP; and maintained at M-phase with CSF. After addition of high concentrations of sperm and nocodazole, CSF was inactivated by calcium to monitor SAC-mediated maintenance of M phase. Time after calcium addition is indicated. Presence of H3T3ph, monitored by Western blot, marks M phase. (B) Immunofluorescence of GFP-xINCENP on sperm chromatin in M-phase extract treated with nocodazole. Green, GFP; purple, DAPI. Bar, 5 µm. (C) Immunofluorescence of GFP-xINCENP (green) on preformed CENP-A chromatin arrays (purple) in M-phase extracts. Bar, 6 µm. (D) Immunofluorescence of GFP or GFP-xSAH on sperm chromatin in M-phase extracts treated with nocodazole. Median, interquartile range (IQR; box), and ±1.5 × IQR (error bars) are shown. Two-tailed Mann–Whitney *t* test; $n = 20$ spreads per sample; ***, $P \leq 0.001$. Bar, 2 µm.

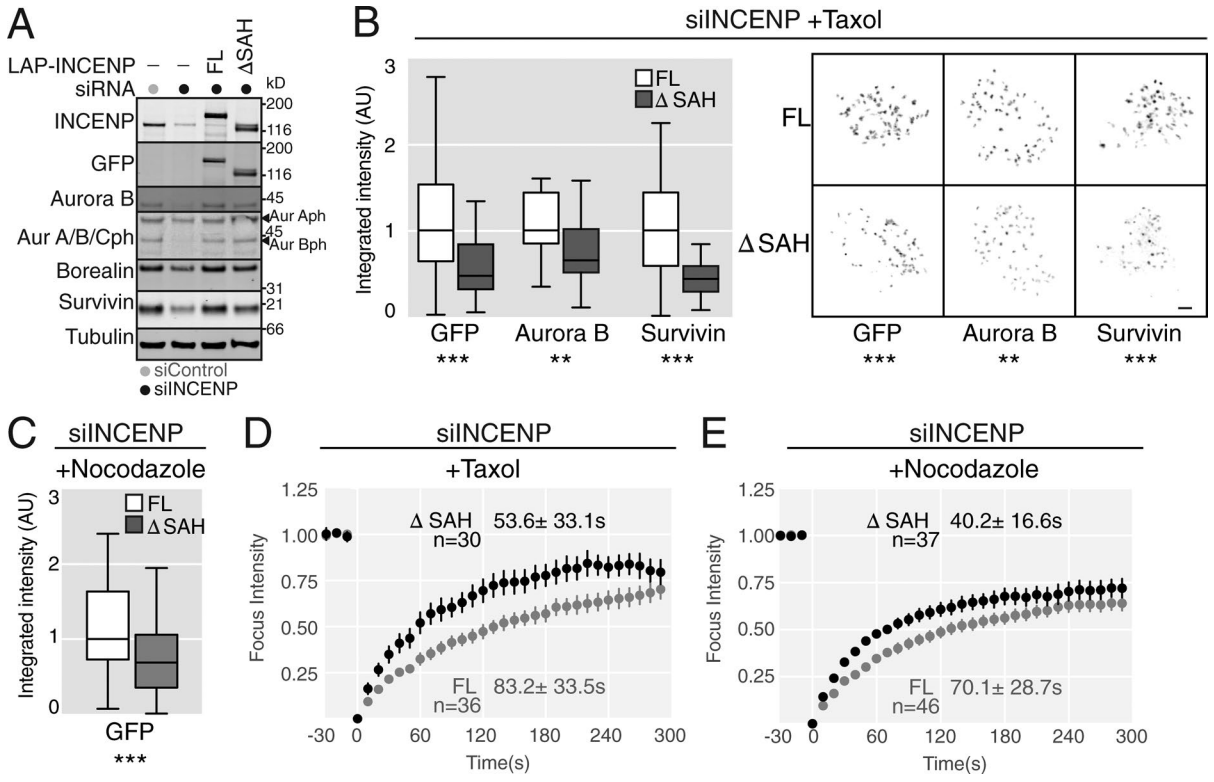

Figure 2. **The SAH domain is required for CPC localization at the centromere in human cells.** (A) Western blot of HeLa cell extracts reconstituted as indicated. Anti–Aurora A/B/Cph detects the phosphorylated T-loop of Aurora A and Aurora B. (B and C) Integrated intensity at the centromere was quantified for each epitope in taxol (B) or nocodazole (C). Data represent $n \geq 28$ cells in B and $n \geq 74$ cells aggregated from three independent experiments for C. Median, IQR (box), and ±1.5 × IQR (error bars) are shown. Two-tailed Mann–Whitney *t* test; **, $P \leq 0.01$; ***, $P \leq 0.001$. Bar, 2 µm. AU, arbitrary units. (D and E) FRAP of centromeric foci in taxol-treated (D) or nocodazole-treated (E) cells reconstituted with hINCENP or hINCENP ΔSAH. The mean FRAP recovery curve with a 95% confidence interval is displayed with the mean $t_{1/2}$ ± SD for each sample; data compiled from $n = 2$ independent experiments per condition, $n \geq 30$ centromeres for each condition.

localized to chromatin even after depletion of endogenous CPC (Fig. S1 A), and endogenous INCENP did not copurify with the 6Myc-tagged xSAH domain (Fig. S1 B). These results indicate that in addition to Survivin and Borealin, the SAH domain interacts with chromatin to support the SAC in *Xenopus* egg extracts.

The SAH domain supports CPC localization at the centromere in human cells

To test whether the SAH domain contributes to centromeric localization of the CPC in human cells, we generated doxycycline-inducible HeLa T-REx cell lines containing full-length human INCENP (hINCENP) or hINCENP ΔSAH. These constructs are resistant to an INCENP siRNA and N-terminally fused to the LAP tag, which contains GFP (Cheeseman and Desai, 2005; Vader et al., 2006). Treating these cells with INC ENP siRNA reduced endogenous INCENP protein levels by 80%, whereas doxycycline induced LAP-hINCENP expression to near-wild-type levels (Fig. 2 A). As previously published (Honda et al., 2003), knockdown of INCENP reduced the abundance of the other CPC subunits, but it was rescued by expressing either hINCENP or hINCENP ΔSAH (Fig. 2 A). Coimmunoprecipitation of CPC subunits with hINCENP ΔSAH confirmed that the SAH domain is dispensable for CPC formation (Fig. S2 A).

hINCENP and hINCENP ΔSAH both showed the appropriate spatiotemporal distribution, including enrichment at the centromere during pro-/metaphase and transfer to the spindle midzone during anaphase (Fig. S2, B and C). Compared with hINCENP, however, hINCENP ΔSAH was less abundant at the centromere and at the spindle midzone, consistent with our observations in *Xenopus* (Fig. 1 B) and the previously published role of the hINCENP SAH domain in midzone localization (Samejima et al., 2015; van der Horst et al., 2015), respectively. Quantitation confirmed that expression of hINCENP ΔSAH significantly reduced the abundance of all tested CPC components at the centromere relative to hINCENP without affecting the number of INCENP-positive centromeres in either nocodazole- or taxol-treated cells (Fig. 2, B and C, and Fig. S2 D). Reduced CPC abundance at the centromere was accompanied by a slight reduction in centromeric H3T3ph and the appearance of H2A T120ph on chromosome arms (Fig. S2 E). These defects are consistent with the idea that reduced CPC abundance causes defects in Aurora B–dependent activation of the H3T3 kinase Haspin and Aurora B–dependent recruitment of the H2A T120 kinase Bub1 to the kinetochore (Carmena et al., 2012).

To determine whether the SAH domain contributes to CPC stability at the centromere, we performed FRAP on hINC ENP or hINCENP ΔSAH foci at the centromere in mitotic cells treated with taxol (Figs. 2 D and S2 F). hINCENP had a mean halftime of recovery ($t_{1/2}$) of 83.2 ± 33.5 s, whereas INCENP ΔSAH had a reduced $t_{1/2}$ (53.6 ± 33.1 s). hINCENP ΔSAH also showed a reduced $t_{1/2}$ in nocodazole-treated cells relative to full-length (FL) hINCENP. Additionally, the maximum intensity of recovery for hINCENP ΔSAH is higher than that of hINCENP

FL, suggesting that a larger fraction of the population is mobile (Figs. 2 E and S2 F). These results suggest that the SAH domain helps the CPC stabilize on centromeric chromatin in both *Xenopus* egg extracts and human somatic cells.

The SAH domain is required for SAC maintenance and mitotic cell death in taxol-treated human cells

A previous study investigating the role of the SAH domain in the SAC used flow cytometry to measure the relative abundance of mitotic cells (Vader et al., 2007). However, that analysis did not determine the duration of the mitotic arrest or how cells exit mitosis. Therefore, we measured the duration of mitosis (DoM) for single cells using live microscopy in the presence of 500 nM taxol, a concentration known to result in the longest DoM in HeLa cells (Yang et al., 2009). We defined the DoM as the time from nuclear envelope breakdown (NEB) to mitotic exit, which occurred by either slippage into interphase or death in mitosis. In taxol, all cells undergoing slippage produced a single, multinucleate cell because of an inability to complete cytokinesis, whereas cells that died in mitosis exhibited dramatic blebbing followed by compaction into a crenulated spherical mass (Fig. S3 A).

Cells treated with control siRNA exhibit a heterogeneous arrest time in taxol, with a median DoM of 18.6 h (Fig. 3 A). Consistent with the CPC being required for SAC maintenance, INCENP siRNA decreased the median DoM to 8.3 h. Although expression of hINCENP fully rescued the DoM (18.7 h), hINC ENP ΔSAH did not (11.1 h), confirming that the SAH domain is required to maintain the SAC in taxol-treated human cells. Treating cells with monastrol, which inhibits spindle bipolarization and activates the SAC (Kapoor et al., 2000), demonstrated a similar requirement for the CPC and the INCENP SAH domain (Fig. 3 B).

To assess how manipulation of INCENP affects mitotic cell fate (slippage or death in mitosis), we aggregated data from at least five independent replicates of our taxol-induced SAC experiment by normalizing the DoM for each construct to the median DoM of hINCENP in the same replicate (Fig. 3 C). We then visualized the normalized DoM by cell fate for each construct. Although the majority of control cells (84%) or those expressing INCENP (71%) died in mitosis, the majority of cells lacking the CPC (75%) or containing INCENP ΔSAH (59%) underwent mitotic slippage. It is known that impairing the SAC shortens the duration of mitotic arrest in taxol, leading to an increased frequency of mitotic exit by slippage (Gascoigne and Taylor, 2008). Our data are consistent with this observation, as cells undergoing mitotic slippage arrested for half as much time in mitosis when expressing hINCENP ΔSAH relative to hINCENP.

To better correlate the DoM with cell fate, we performed a linear regression of the median DoM against cell survival for every construct in every experiment in this article, in addition to experiments not depicted (Fig. S3 B). We saw a strong, positive correlation between the median DoM of a sample and the percentage of cells dying in mitosis in that sample. The DoM of cells that die in mitosis was relatively constant, indicating that the probability of mitotic cell death, but not the timing of cell death, strongly correlates with the capacity of INCENP to hold the SAC. Thus, the CPC and the INCENP SAH domain ensure a robust SAC response in taxol, which promotes mitotic death.

The SAH domain is required for SAC protein recruitment and kinetochore phosphorylation in taxol-treated human cells

Next, we investigated the importance of the SAH domain in recruiting SAC regulators to the kinetochore. Although it was reported that BubR1 recruitment is qualitatively not affected by deleting the SAH domain in U2OS cells (Vader et al., 2007), HeLa cells expressing INCENP ΔSAH exhibited a quantitative reduction in the amount of Mad1, Bub1, and BubR1 at the kinetochore compared with hINCENP (Fig. 3 D), without affecting the number of Bub1/BubR1-positive kinetochores (Fig. S2 D). hINCENP ΔSAH showed no defect in recruitment of CENP-A or Hec1 (Fig. S3 C) or in Aurora B–dependent phosphorylation of CENP-A at the centromere or H3S10 on chromatin (Fig. 3 E). However, hINCENP ΔSAH had a reduced amount of phosphorylation on kinetochore substrates implicated in kMT stability and SAC maintenance, such as Dsn1 S100ph, KNL1 S24ph, and Hec1 S44ph (Hsu et al., 2000; Zeitlin et al., 2001; Welburn et al., 2010; DeLuca et al., 2011; Fig. 3, E and F; and Fig. S3 D). These results, together with a previous study (Samejima et al., 2015), suggest that the SAH domain can promote the SAC by supporting Aurora B–dependent kinetochore phosphorylation and SAC protein recruitment.

Neither cytoplasmic activation of Aurora B nor tethering of INCENP to the centromere/kinetochore is sufficient to support the SAC

A study in budding yeast has suggested that centromere targeting of the CPC is not required for its functions, including SAC activation, if Aurora B is activated by an alternative mechanism such as binding to MT (Campbell and Desai, 2013). Thus, we tested whether artificial activation of Aurora B by forced dimerization could bypass the requirement of the SAH domain for the SAC. As previously shown in *Xenopus* egg extracts (Tseng et al., 2010), replacing the SAH domain with the dimerization domain of GCN4 (hINCENP ΔSAH ∇GCN4) dramatically increased the overall level of Aurora B autophosphorylation in human cells (Fig. 4, A and B). However, this construct phenocopied hINCENP ΔSAH, failing to rescue the defect in INCENP centromeric localization (Fig. S3 E), kinetochore phosphorylation (Fig. S3 E), and the SAC (Fig. 4 C). These results suggest that cytoplasmic activation of Aurora B is insufficient to support the SAC in taxol.

We next tested whether tethering INCENP to the centromere or the kinetochore bypasses the requirement of the SAH domain. We generated HeLa cell lines in which the N-terminal CEN domain of INCENP was replaced with one of the following targeting modules: FL human Mis12 (Mis12-hINCENP ΔCEN) for kinetochore targeting, FL CENP-B (CB-hINCENP ΔCEN) for stable centromere targeting, or CENP-B DNA binding domain (CB^{DBD}-hINCENP ΔCEN) for more dynamic centromere targeting (Fig. 4 D; Liu et al., 2009; Wang et al., 2011). We then depleted endogenous INCENP, expressed the targeting chimeras, and monitored the DoM of these cells in taxol by live imaging (Fig. 4 E). Consistent with the requirement of the Survivin–H3T3ph interaction in SAC maintenance in human cells (Lens et al., 2006; Wang et al., 2010), hINCENP ΔCEN had a significantly shorter DoM than cells treated with siINCENP alone, likely because of hINCENP ΔCEN sequestering Aurora B from remaining endogenous INCENP protein. Surprisingly,

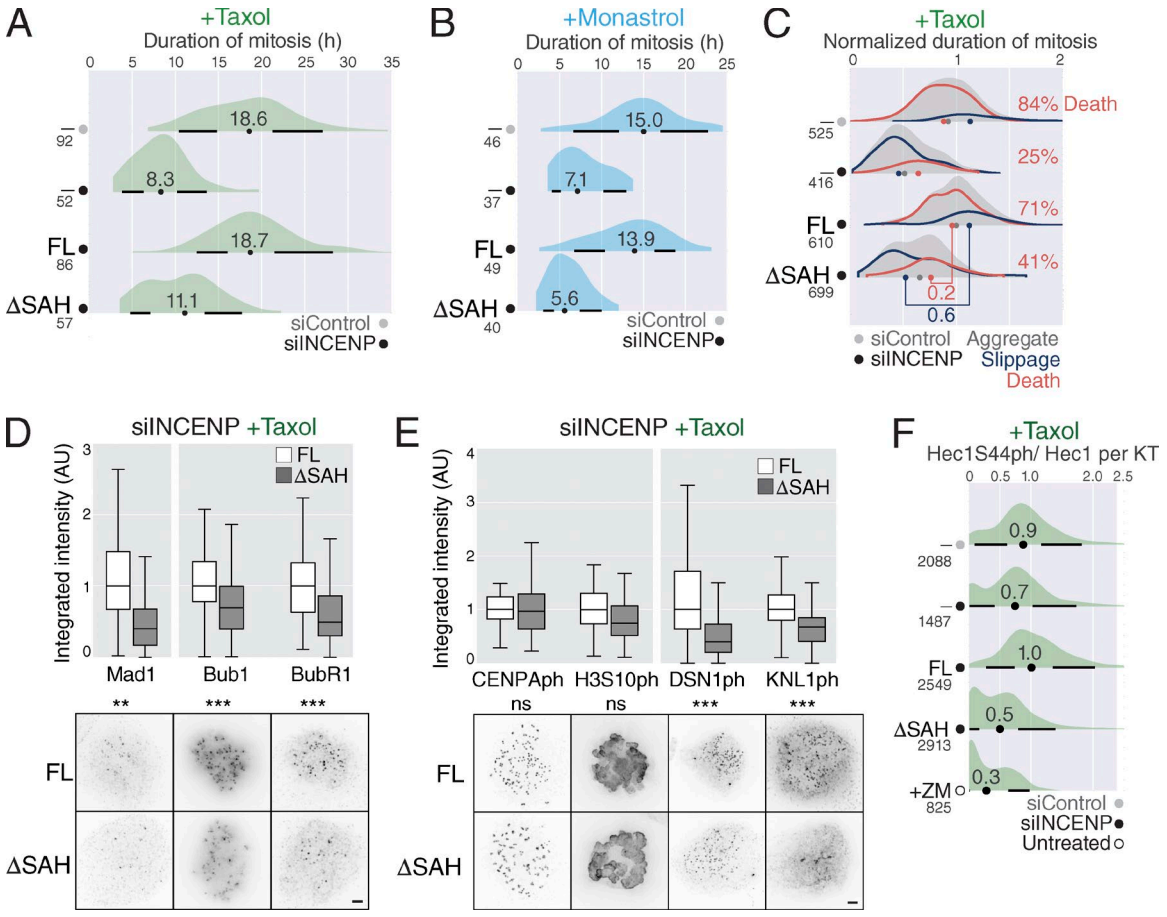

Figure 3. **The SAH domain is required for the SAC and kinetochore phosphorylation in human cells.** (A) DoM for HeLa cells with taxol, pretreated with control siRNA or INCENP siRNA and complemented with hINCENP FL or hINCENP-ΔSAH (ΔSAH). Data are displayed as a kernel density estimate of DoM for all cells in each condition. A box plot with a circle at the median and whiskers extending to ±1.5 × IQR is under each density, *n* values indicated under sample name, siRNA treatment indicated by gray (siControl) or black (siINCENP) circles adjacent to the sample name. (B) Same as A, except cells were treated with monastrol. (C) Normalized DoM for all cells (gray) and for cells undergoing death in mitosis (red) or mitotic slippage (blue). Data aggregated from at least five independent experiments. All values were normalized to the median of hINCENP in that experiment. Maximum height of each curve is proportional to percentage composition of that class in the aggregate. Red numbers on the right indicate the overall percentage of cells dying in mitosis. The difference in the normalized DoM between cells complemented with FL or ΔSAH hINCENP is also indicated. (D and E) Immunofluorescence quantification of SAC proteins (D) and Aurora B–dependent phosphorylation (E) in taxol-treated cells. In D, the data represent integrated intensity at the kinetochore from $n \geq 18$ cells for Mad1 and $n \geq 86$ cells aggregated from three independent experiments for Bub1 and BubR1. In E, the data represent integrated intensity at the centromere for $n \geq 52$ cells aggregated from two experiments for CENP-A S7ph, integrated intensity on chromatin for $n \geq 20$ cells for H3S10ph, and $n \geq 1{,}800$ individual kinetochore measurements for Dsn1 S100ph and Knl1 S24ph using a marker epitope. Representative images approximating the median are presented. Median, IQR (box), and ±1.5 × IQR (error bars) are shown. Two-tailed Mann–Whitney *t* test; ns, not significant; **, $P \leq 0.01$; ***, $P \leq 0.001$. Bars, 2 µm. (F) Immunofluorescence quantification of Hec1 S44ph at individual kinetochores standardized to total Hec1 at that kinetochore. Data are visualized as a kernel density estimate, *n* values indicated under the sample name. ZM, Aurora B inhibitor ZM447439. The maximum height of the density for ZM-treated cells was scaled independently.

none of the INCENP-targeting chimeras supported a robust SAC response. The DoM of cells in which INCENP was targeted to CENP-B chromatin or the kinetochores was longer than the DoM of cells expressing hINCENP ΔCEN but similar to the DoM of cells treated with siINCENP alone. These data demonstrate that targeting INCENP to the centromere or the kinetochore cannot fully bypass the requirement of the CEN domain.

Failure of these chimeric constructs to support the SAC was unexpected, because they are known to promote kMT destabilization and induce a mitotic delay when expressed on top of endogenous INCENP (Liu et al., 2009; Wang et al., 2011). Consistent with these published results, when expressed on top of endogenous INCENP in the absence of any MT poisons, Mis12-hINCENP ΔCEN caused the mitotic delay much more effectively than hINCENP ΔCEN (Fig. 4 F), whereas overexpression of hINCENP did not induce any mitotic delay (Fig. S3 F). Notably, the untagged version of hINCENP ΔCEN ΔSAH was not as potent as hINCENP ΔCEN, but the effect of Mis12-hINCENP ΔCEN ΔSAH was comparable to that of Mis12-hINCENP ΔCEN. These results indicate that the SAH domain of INCENP that is stably associated with the kinetochore is dispensable for SAC activation.

INCENP MT binding is negatively regulated by mitotic phosphorylation in the regions flanking the SAH domain

Aurora B is critical in human cells for the SAC in the presence of MTs (taxol, monastrol) but less important in the absence of MTs (nocodazole; Ditchfield et al., 2003; Hauf et al., 2003; Santaguida et al., 2011). Therefore, we wondered whether the MT-binding capacity of the SAH domain contributes to the SAC. As a first step, we tested whether a particular region of

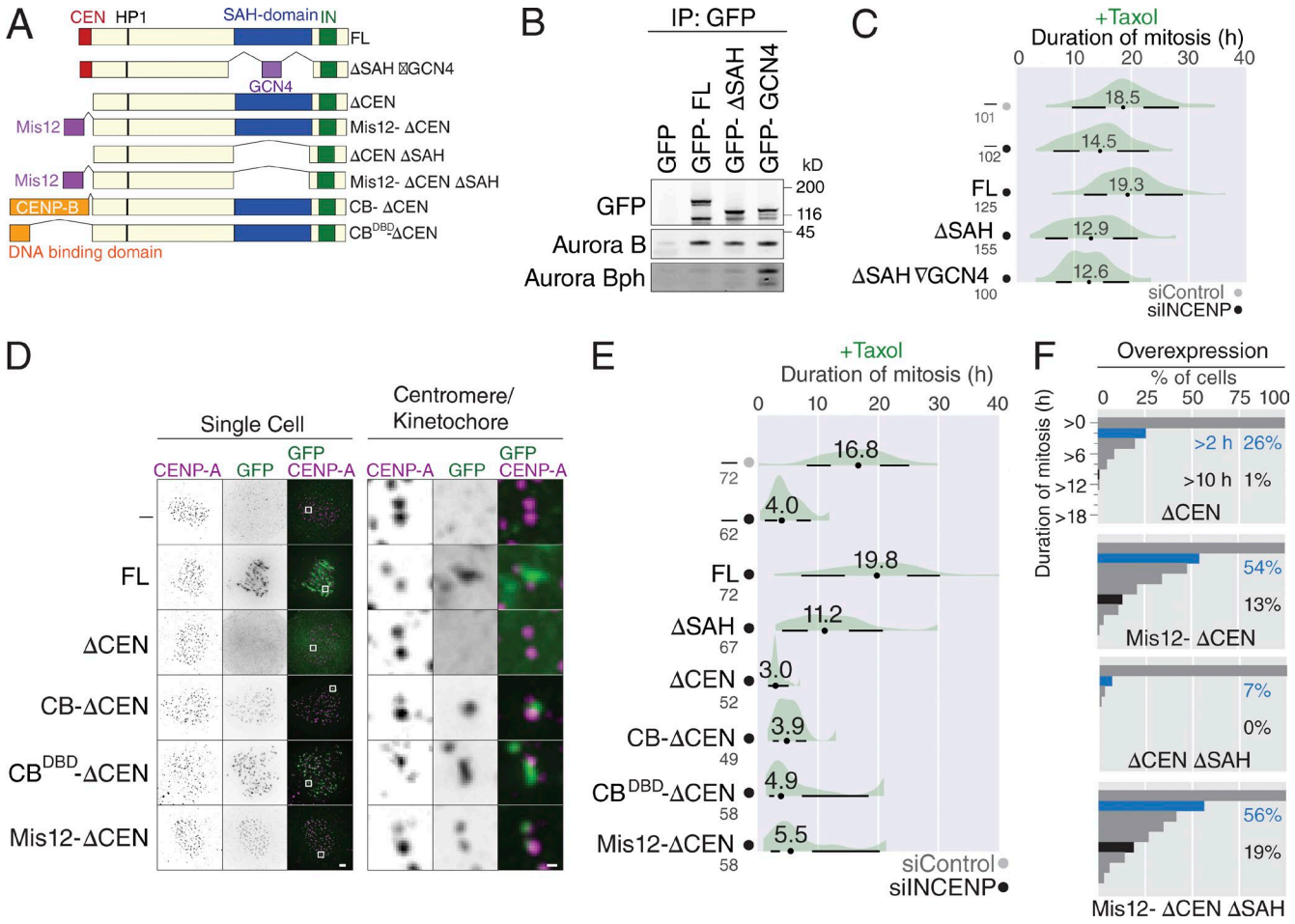

Figure 4. **Clustering or kinetochore targeting of the CPC is insufficient to support the SAC.** (A) Diagram of LAP-tagged hINCENP constructs. (B) Western blot of anti-GFP immunoprecipitation (IP) of the indicated constructs from mitotic HeLa cell extracts. (C) DoM for cells in taxol. Representative of $n = 2$ independent experiments. (D) Immunofluorescence of various INCENP constructs. Each construct was expressed over endogenous INCENP. For each construct, the left three panels are single-cell images; the right three are zoom-ins of a representative kinetochore pair indicated by white boxes. Bars: (single cell) 2 µm; (centromere/kinetochore) 0.25 µm. (E) DoM for cells in taxol. The maximum height for the density estimate of hINCENP ΔCEN was scaled independently. Representative of $n = 2$ independent experiments. (F) Each construct was expressed over endogenous INCENP and synchronized at the G2/M transition by treatment with the Cdk1-inhibitor RO-3306. After washout of the inhibitor, cells synchronously entered mitosis. Plots show the cumulative minimum DoM for each construct. Blue bars, arrested for at least 2 h; black bars, arrested for at least 10 h; $n \geq 90$ cells per sample.

the SAH domain contributes to MT binding using *Xenopus* egg extracts and found that 6Myc-tagged xSAH domain localized to the spindle with particular enrichment at the spindle poles (Fig. S4 A). Using a series of deletions, we mapped this spindle binding activity to the first ∼100 aa of the SAH domain. We also identified a shorter 35-aa deletion in the N terminus of the xSAH domain (ΔSAH^{N}) that was unable to bind the spindle. Thus, the N terminus of the *Xenopus* SAH domain binds the spindle, consistent with reports for the SAH domain of human and chicken (Samejima et al., 2015; van der Horst et al., 2015).

Spindle pole enrichment of the xSAH domain is distinct from xINCENP, which localizes along the entire spindle (Tseng et al., 2010). Searching for elements flanking the SAH domain that might account for this difference, we identified four putative Cdk-dependent phosphorylation sites ([S/T]P) upstream of the SAH domain and two sites downstream of the SAH domain that are widely conserved among vertebrates species, and thus we named these flanking regions phospho-regulatory domain (PRD) 1 and 2, respectively (Figs. 5 A and S4 B).

To determine whether these putative Cdk sites are phosphorylated in *Xenopus* egg extracts, we prepared a fragment encompassing PRD1, SAH, and PRD2 (PRD-xSAH), as well as versions in which the six conserved putative Cdk sites, in addition to one SP site in PRD1 not conserved in humans, were made unphosphorylatable by mutation to alanine (PRD-xSAH 7A) or phosphomimetic by mutation to aspartate (PRD-xSAH 7D; Fig. 5 A). These fragments were incubated in M-phase or interphase extracts, followed by treatment with or without phosphatases (Fig. 5 B). Although the gel migration pattern of xSAH domain alone was not affected by cell-cycle stage or phosphatase treatment, the PRD-xSAH fragment in M phase ran as a smear that collapsed to a single band upon phosphatase treatment, indicative of phosphorylation. The mobility shift of this fragment was greatly reduced in interphase, suggesting that these [S/T] P sites are phosphorylated only in metaphase. Furthermore, the PRD-xSAH 7D fragment ran at the same size as the upper smear of PRD-xSAH, and the PRD-xSAH 7A mutant ran at a similar size to the PRD-xSAH upon phosphatase treatment.

To examine whether phosphorylation of the PRD regulates MT binding, the localization of the PRD-xSAH fragments

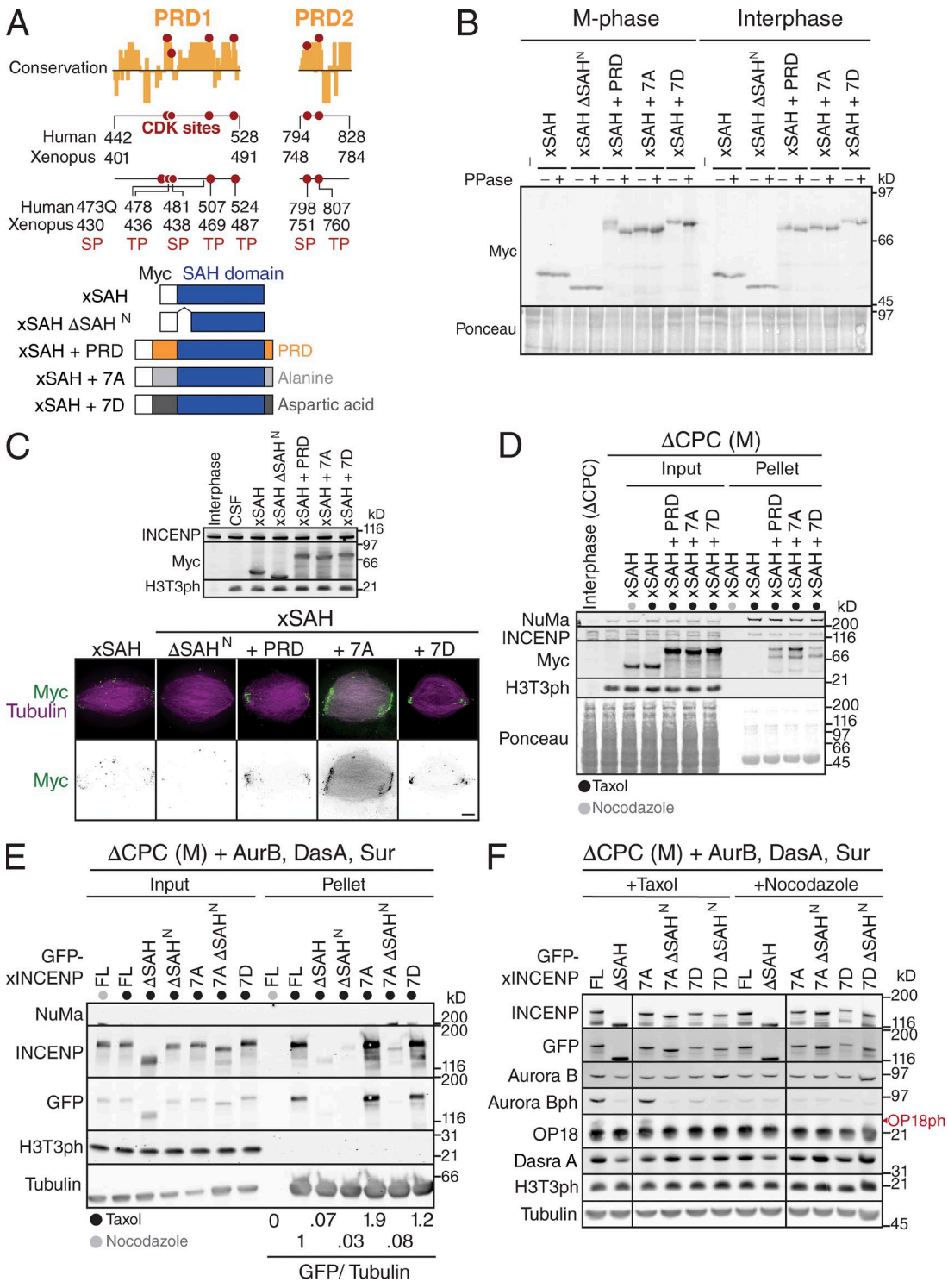

Figure 5. **MT binding of the SAH domain is negatively regulated by phosphorylation.** (A) Conservation of each residue in the PRDs relative to the mean conservation of residues in INCENP (top). Conservation was determined using conSURF (Landau et al., 2005) with 25 vertebrate INCENP homologs (Fig. S4 B). Putative Cdk sites conserved in at least 22 species are indicated (red circles). Diagrams of 6Myc-tagged constructs used in B, C, and D (bottom). (B) Western blot of various Myc-tagged xSAH domain constructs expressed in *Xenopus* egg extracts. Samples were either taken from extracts (–) or diluted in buffer containing lambda phosphatase and incubated at 30°C for 40 min (+). (C) Immunofluorescence of the indicated Myc-tagged constructs on the spindle in M-phase *Xenopus* egg extract (bottom). Western blot shows equal protein expression (top). Bar, 5 µm. (D) MT pelleting assay with the indicated constructs after depletion of endogenous INCENP. M-phase egg extract was incubated with nocodazole (gray circle) or taxol (black circles) for 30 min, and MT pellets were analyzed by Western blot. (E) MT pelleting assay as in D in extract reconstituted with the indicated GFP-xINCENP construct, xAurora B, xDasra A, and xSurvivin. Quantitation of pelleted GFP-xINCENP constructs relative to pelleted tubulin was performed in ImageJ and is shown at the bottom. (F) Western blot visualizing the MT-dependent activation of Aurora B. M-phase extract was reconstituted with the indicated INCENP constructs and then incubated in the presence of the indicated drug for 40 min. Aurora B activation was assessed by the appearance of Aurora B autophosphorylation (Aurora Bph) and OP18 hyperphosphorylation (OP18ph).

on the spindle was assessed in M-phase egg extracts. Although the xSAH domain only weakly bound the spindle pole, the PRD-xSAH 7A mutant was highly enriched on the spindle and spindle pole (Fig. 5 C). The PRD-xSAH 7D mutant and the PRD-xSAH fragment localized to the spindle pole only slightly better than the xSAH domain alone. Furthermore, MT cosedimentation assays showed that the SAH domain exhibited little to no MT binding in the absence of the PRD (Fig. 5 D). The PRD-xSAH 7A fragment exhibited a twofold increase in sedimentation with MTs compared with PRD-xSAH. These results indicate that the PRD and SAH domain promote MT binding, which is negatively regulated by Cdk-dependent phosphorylation at the PRD.

To test whether the PRD regulates the MT binding of xINCENP FL, we generated versions of GFP- xINCENP containing the phospho-null (xINCENP 7A) and phospho-mimetic (xINCENP 7D) mutations either alone or in combination with the 35-aa deletion that abrogates the MT binding capacity of the SAH domain (ΔSAH^N). M-phase ΔCPC extracts were reconstituted with the CPC containing these INCENP constructs, and the MT cosedimentation assay was performed (Fig. 5 E). Although xINCENP demonstrated robust MT binding, this was dramatically reduced in xINCENP ΔSAH and xINCENP ΔSAH^N. xINCENP 7A showed an almost twofold increase in MT binding, whereas xINCENP 7D bound to MTs similarly to xINCENP. Incorporating ΔSAH^N into INCENP 7A abrogated MT binding, suggesting that the PRD is insufficient to support MT binding in the absence of the SAH domain.

We have previously shown that MTs assembled by taxol in *Xenopus* egg extracts activate Aurora B in a manner dependent on the SAH (Tseng et al., 2010). Indeed, the CPC reconstituted with xINCENP and xINCENP 7A exhibited robust Aurora B autophosphorylation (Fig. 5 F). However, deleting the MT-binding region of the SAH domain (xINCENP ΔSAH, ΔSAH^N, or 7A ΔSAH^N) or xINCENP 7D prevented MT-dependent activation of Aurora B. These results indicate that the SAH^N region and dephosphorylation of the PRD are required for MT-dependent activation of Aurora B.

The SAH domain binds MTs to maintain the SAC in taxol-treated cells

In *Xenopus* egg extracts, INCENP is still functional in spindle assembly when the SAH domain is replaced with an exogenous MT-binding domain (MTBD; Tseng et al., 2010). We adopted a similar strategy to determine whether the SAH domain binds MTs to sustain the SAC in taxol-treated HeLa cells. We replaced the SAH domain with the MTBD from MAP4 (hINCENP ΔSAH ∇MAP4; Fig. 6 A) and confirmed that this construct localized to both MTs and chromatin (Fig. 6 B). Although the median DoM for hINCENP ΔSAH in taxol was 10.9 h, hINCENP ΔSAH ∇MAP4 partially rescued this defect with a median DoM of 13.6 h and completely rescued the defect in mitotic cell fate and BubR1 localization (Fig. 6, C and D), suggesting that the SAH domain supports the SAC through MT binding.

Given that the SAH domain interacts with both chromatin and MTs, we sought to more precisely disrupt MT binding by deleting the 35 aa in the N terminus of the INCENP SAH domain required for MT binding in *Xenopus* (hINCENP ΔSAH^N). Although hINCENP had a median DoM of 16.6 h, hINCENP ΔSAH^N arrested for 12.9 h (Fig. 6 C). Several lines of evidence indicate that this defect was a result of attenuated MT-binding activity, rather than a defect in chromatin binding or the length of the SAH domain. First, the levels of hINCENP ΔSAH^N at the centromere were indistinguishable from those of hINCENP (Fig. S3 E). Second, two larger deletions (47 and 107 aa) in the SAH domain downstream of the MT-binding region caused a relatively minor reduction in DoM compared with the 35-aa deletion in ΔSAH^N (Fig. S5 A). Third, replacing the N terminus of the SAH domain with the MAP4-MTBD (hINCENP ΔSAH^N ∇MAP4) completely rescued the SAC defect (Fig. 6 C). Finally, although the SAH domain was required for BubR1 recruitment and Dsn1 S100ph at the kinetochore in taxol (Fig. 3, D and E), it became dispensable when MTs were depolymerized using nocodazole (Fig. 6 E). hINCENP ΔSAH also supported relatively higher levels of Hec1 S44ph at the kinetochore in nocodazole (Fig. 6 F) than in taxol (Fig. 3 F), whereas the levels of KNL1 S24ph and Bub1 recruitment were similarly defective in both conditions (Fig. 3, D and E, and Fig. 6 E). These observations are consistent with the idea that human INCENP binding to MTs through its SAH domain supports kinetochore phosphorylation and checkpoint activation in the presence of MTs.

INCENP PRD phosphorylation attenuates MT binding and the SAC in human cells

To test the functional significance of PRD phosphorylation, which suppresses MT binding of the SAH domain, we treated HeLa cells with siRNA against endogenous hINCENP and induced the expression of mutants in which Cdk sites in the PRD were mutated to alanine (hINCENP 6A) or the phosphomimetic aspartate (hINCENP 6D; Fig. 7 A). As predicted, hINCENP 6A localized prominently to MTs, whereas hINCENP and hINCENP 6D did not (Fig. 7, B–D). Expression of hINCENP 6A caused a mitotic delay without any MT poisons, driven by an increase in the time from metaphase alignment to anaphase onset, whereas constructs defective in MT binding (6D and ΔSAH) initiated anaphase in slightly less time than hINCENP (Figs. 7 D and S5 B). In the presence of taxol, the DoM of hINCENP 6A was significantly longer than that of hINCENP 6D, which phenocopied the SAC defect of hINCENP ΔSAH and ΔSAH^N (Fig. 7 E). These results indicate that the capacity of INCENP to support the SAC can be regulated by PRD phosphorylation status, such that PRD phosphorylation attenuates MT binding and promotes SAC silencing.

Finally, we asked whether hINCENP MT binding could support the taxol-mediated SAC independent of chromatin binding. We deleted the hINCENP CEN domain and mutated the PRD to alanine (hINCENP ΔCEN 6A), which enhances MT binding, or aspartate (hINCENP ΔCEN 6D; Fig. 7 A). As we saw previously (Fig. 4 E), expression of hINCENP ΔCEN reduced the median DoM relative to INCENP siRNA alone from 8.6 to 4.3 h (Fig. 7 F). hINCENP ΔCEN 6A interacted with the spindle and modestly increased the DoM to 5.8 h. This increase was dependent on MT binding, as the same construct with a deletion in the N terminus of the SAH domain (hINCENP ΔCEN 6A ΔSAH^N) bound weakly to the spindle and had a median DoM of 4 h. Furthermore, hINCENP ΔCEN 6D had a median DoM identical to that of hINCENP ΔCEN. Collectively, these results suggest that targeting INCENP to the mitotic spindle can contribute to SAC maintenance independently of binding to chromatin, though it is insufficient to fully support the SAC without the CEN domain of INCENP.

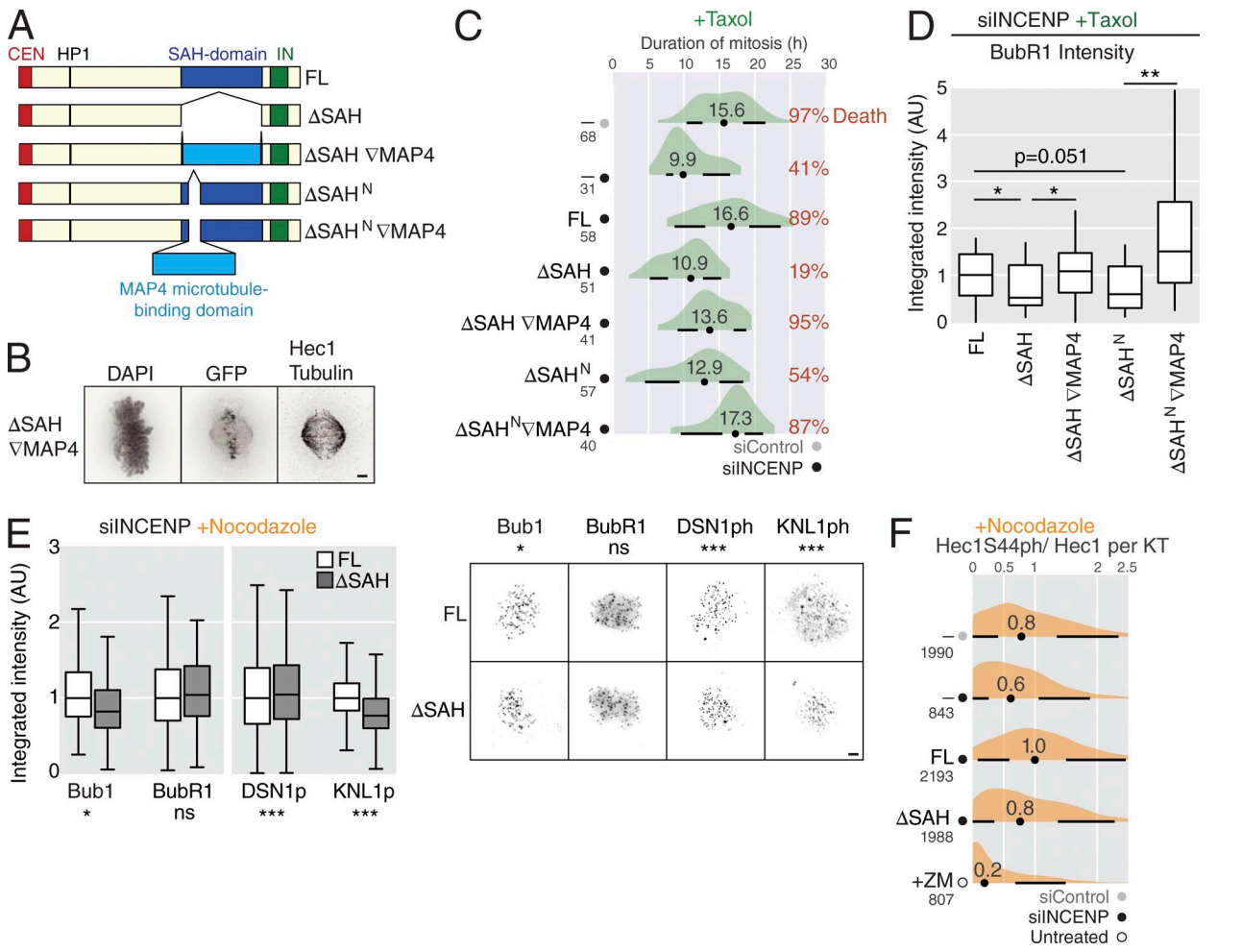

Figure 6. **The SAH domain binds MTs to sustain the SAC.** (A) LAP-tagged hINCENP constructs. (B) Immunofluorescence of hINCENP ΔSAH∇MAP4 expressed over endogenous INCENP in asynchronous HeLa cells. Bar, 2 µm. (C) DoM for cells in taxol. Red values are the percentage cell death for each construct. (D and E) Immunofluorescence quantification of BubR1 in taxol-treated cells (D) and SAC proteins and Aurora B–dependent phosphorylation in nocodazole-treated cells (E) expressing the indicated constructs. In D, the data represent integrated intensity at the kinetochore from $n \geq 27$ cells. In E, the data represent integrated intensity at the kinetochore from $n \geq 54$ cells aggregated from three independent experiments for Bub1 and BubR1, and $n \geq 1{,}720$ individual kinetochore measurements for Dsn1 S100ph and Knl1 S24ph using a marker epitope. Representative images approximate the median. Two-tailed Mann–Whitney *t* test; ns, not significant; *, $P \leq 0.05$; **, $P \leq 0.01$; ***, $P \leq 0.001$. Bar, 2 µm. (F) Immunofluorescence quantification of Hec1 S44ph at individual kinetochores standardized to total Hec1 at that kinetochore for cells treated with nocodazole. The data are visualized as a kernel density estimate, *n* values indicated under the sample name. ZM, the Aurora B inhibitor ZM447439. The maximum height of the density for ZM-treated cells was scaled independently.

Discussion

The INCENP SAH domain maintains the CPC on chromatin

Here we demonstrate that in addition to Survivin and Borealin, which interact with the INCENP CEN domain, the INCENP SAH domain contributes to recruitment of the CPC to the centromere in both *Xenopus* egg extract and HeLa cells (Fig. 8). Deleting the SAH domain reduces CPC abundance and enhances its dynamics at the centromere even in the absence of MTs, indicating that this function is independent of the previously suggested role for the Aurora B–MT interaction in CPC enrichment at the centromere (Banerjee et al., 2014; Krupina et al., 2016). Given that the GFP-tagged xSAH domain is broadly distributed along sperm chromatin in *Xenopus* egg extract in the absence of MTs (Fig. 1 D), the SAH domain may enhance the affinity of the CPC for chromatin.

Although centromere targeting of the CPC is dispensable in budding yeast (Campbell and Desai, 2013), the INCENP CEN domain is required for robust SAC maintenance in human cells (Fig. 4 E), and the SAH domain promotes the SAC in nocodazole-treated *Xenopus* egg extracts (Fig. 1 A). However, artificially targeting INCENP ΔCEN to the centromere (CENP-B fusion) or the kinetochore (Mis12 fusion) did not bypass the requirement for the CEN domain in the taxol-induced SAC (Fig. 4 E). This may be caused by a defect in chromatin-dependent Aurora B activation, which may require a process beyond chromatin targeting, perhaps involving Borealin-mediated dimerization (Bourhis et al., 2009; Bekier et al., 2015; van der Horst et al., 2015). However, even though INCENP dimerization by GCN4 induced Aurora B autoactivation (Fig. 4 B; Tseng et al., 2010), this did not bypass the requirement for the SAH domain in the SAC maintenance, suggesting that activation of Aurora B is insufficient

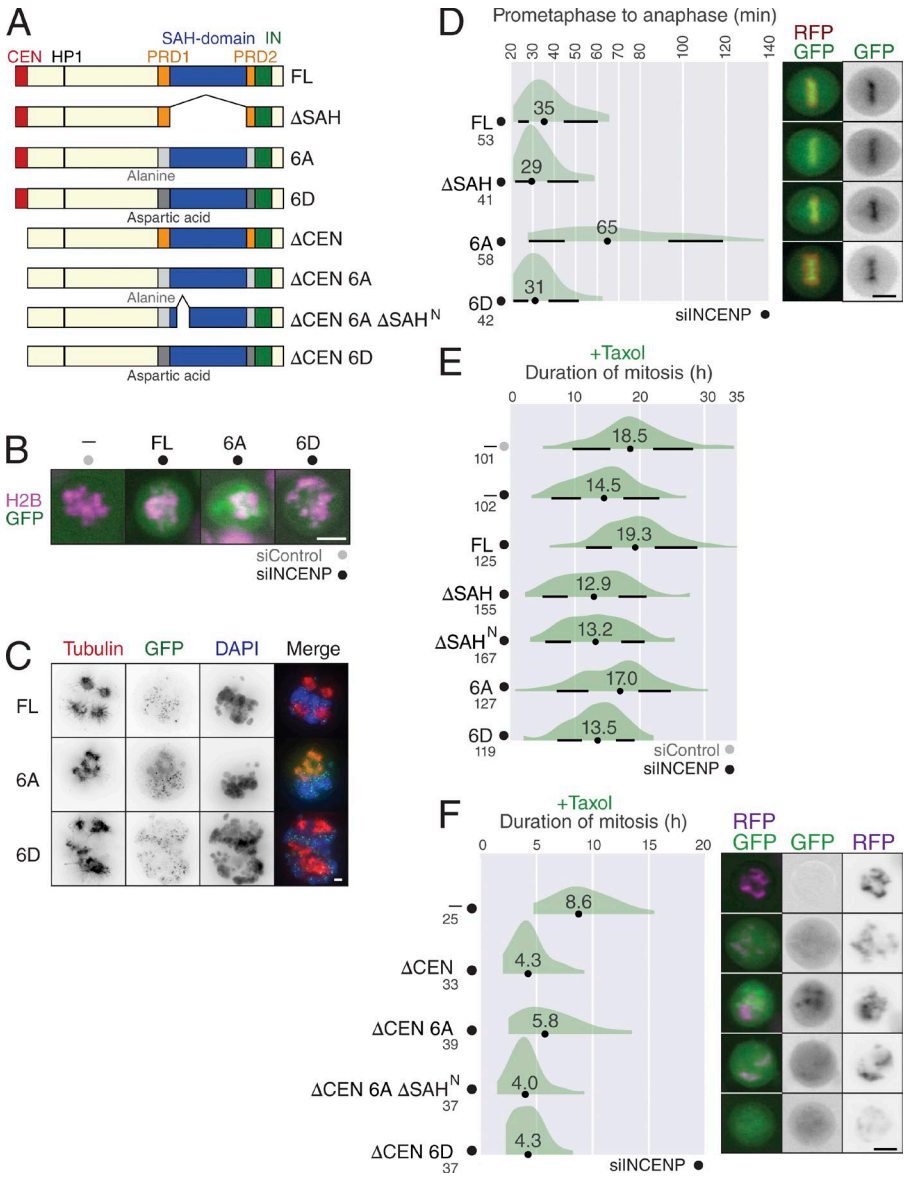

Figure 7. **PRD phosphorylation regulates INCENP MT binding and the SAC.** (A) LAP-tagged hINCENP constructs. (B) Fluorescence images of cells expressing the indicated hINCENP constructs in taxol after knockdown of endogenous INCENP. Taken from a live imaging experiment. Green, GFP-INCENP; purple, RFP-H2B. Bar, 10 µm. (C) Immunofluorescence of the indicated constructs expressed over endogenous INCENP in cells treated with taxol. Bar, 2 µm. (D) DoM for cells undergoing unperturbed mitosis (left) and representative fluorescence images from the live imaging experiment (right). Representative of $n = 3$ independent experiments. Green, GFP-INCENP; red, RFP-H2B. Bar, 10 µm. (E) DoM for cells in taxol. Data were collected from the same experiment as Fig. 4 C. Representative of $n = 3$ independent experiments. (F) DoM for cells in taxol (left) and representative fluorescence images from the live imaging experiment (right). Green, GFP-INCENP; purple, RFP-H2B. Data from a single experiment. Bar, 10 µm.

to support its function at the centromere/kinetochore in the absence of the SAH domain.

The INCENP SAH domain binds MTs to support the SAC in taxol-treated cells

Consistent with previous studies (Samejima et al., 2015; van der Horst et al., 2015), we have shown that the N-terminal segment of the SAH domain is critical for MT binding. The MAP4 MTBD bypassed the requirement of this segment (Fig. 6 C), suggesting that the MT-binding capacity of the SAH domain is important for SAC activation/maintenance in response to the aberrant kMT attachments generated by taxol or monastrol.

The SAH–MT interaction could promote the SAC through several mechanisms. First, as previously reported

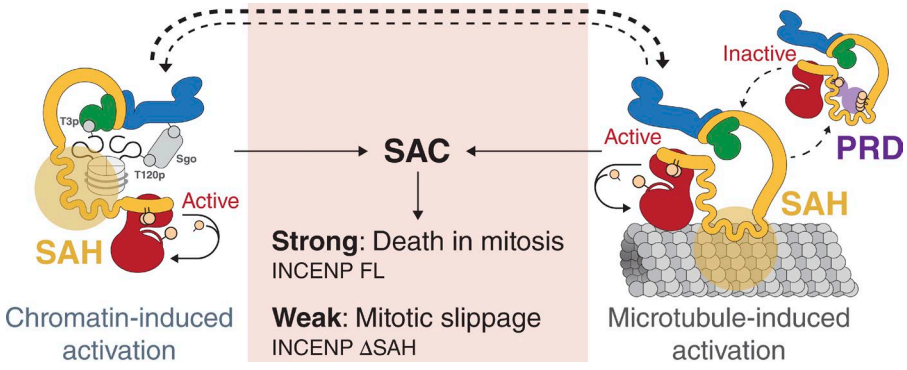

Figure 8. **Model for the role of the CPC in the SAC.** The SAH domain supports an interaction with chromatin to stabilize the CPC at the centromere (left). Similarly, the SAH domain mediates direct binding to MTs and MT-dependent activation of Aurora B (right). The MT–CPC interaction is suppressed by Cdk-dependent phosphorylation at the PRD of INCENP (top right). After activation, Aurora B may diffuse and phosphorylate substrates at the kinetochore/centromere/kMT (middle) to support SAC activation/maintenance. CPC subunits are Aurora B (red), INCENP (yellow), Survivin (green), and Borealin (blue).

(Banerjee et al., 2014; Krupina et al., 2016), CPC–MT interaction may facilitate CPC enrichment at the centromere. However, this is unlikely to be the sole mechanism, as a 35-aa deletion in the MT-binding region (hINCENP ΔSAH^N) attenuated the SAC without affecting localization to the centromere (Figs. 7 and S5 A). Second, the INCENP SAH domain may support MT-dependent activation of Aurora B (Fig. 5 F; Tseng et al., 2010). Centromeric enrichment of the CPC may enhance the accessibility of the CPC to local kMTs, where Aurora B is activated to phosphorylate kinetochore substrates. Third, SAH–MT binding may support effective phosphorylation of MT-binding proteins, such as Hec1, the Ska complex, mDia3, and EB2, to destabilize kMT attachment (Cheng et al., 2011; DeLuca et al., 2011; Chan et al., 2012; Iimori et al., 2016). Consistent with this model, Aurora B–dependent phosphorylation can be detected on the mitotic spindle (Tseng et al., 2010), and the INC ENP–MT interaction preferentially promotes Aurora B–dependent phosphorylation of MT-bound substrates over unbound substrates in vitro (Banerjee et al., 2014). This may be related to the fact that Aurora B is a basophilic kinase (Alexander et al., 2011), and that the basic residues of MTBDs, such as those at the Hec1 N-terminal tail and the SAH, commonly interact with the negatively charged E-hooks of tubulin (Alushin et al., 2010; van der Horst et al., 2015). Because kMT attachments are stabilized by tension independently of Aurora B (Akiyoshi et al., 2010), the SAH domain may competitively displace MTBDs at the kinetochore from MTs to facilitate their phosphorylation by Aurora B preferentially at the kinetochore with no tension. Our observation that the SAH is dispensable for ectopic SAC activation by kinetochore targeting is consistent with the idea that the SAH increases Aurora B substrate accessibility, because stabilizing INCENP at the kinetochore would facilitate this in a manner independent of MT-binding (Fig. 4 F). However, the possibility that the SAH domain facilitates Aurora B substrate recognition independently of MT or chromatin binding may not be ruled out. Minor contributions to the SAC by the C-terminal SAH segment that is not supporting MT binding may reflect such functions (Fig. S5 A).

Although the SAH–MT interaction supports the SAC, it is not sufficient for a robust mitotic arrest in the absence of the CEN domain (Fig. 7 F). We propose that the CPC must interact with both centromeric chromatin and MTs to support a robust SAC arrest (Fig. 8).

Cdk-dependent regulation of the INCENP SAH domain

In budding yeast, phosphorylation of the INCENP homologue Sli15 by Cdk1 prevents binding to the mitotic spindle before anaphase (Pereira and Schiebel, 2003). These Cdk1 phosphorylation sites are also enriched in the region upstream of the putative coiled-coil (or SAH) domain in Sli15 (Pereira and Schiebel, 2003), similar to vertebrate INCENP homologs. However, there is a conflict in the literature as to whether phosphorylation of Sli15 supports or inhibits the SAC (Mirchenko and Uhlmann, 2010; Makrantoni et al., 2014). In human cells, Cdk1-dependent phosphorylation at T59 of INCENP indirectly inhibits CPC binding to the spindle by preventing it from binding to MKLP2 (Hümmer and Mayer, 2009). Here, we demonstrate that the PRD enhances SAH-dependent MT binding and that Cdk-dependent phosphorylation of the PRD reduces the binding of INCENP to MTs (Figs. 4 and 8). Furthermore, our data suggest that whereas the SAH–MT interaction contributes to SAC activation in taxol (Fig. 7 E), suppressing the SAH–MT interaction by phosphorylation of the PRD is required to silence the SAC after metaphase alignment of chromosomes during an unperturbed mitosis (Fig. 7 D), although it is possible that INCENP 6A supports metaphase alignment without bipolar attachment (Kapoor et al., 2006).

Because Cdk1–Cyclin B activity is high in early mitosis, it may be counterintuitive that dephosphorylation of the PRD helps sustain the SAC. However, the INCENP PRD may be targeted for context-dependent dephosphorylation to locally regulate Aurora B activity. At the outer kinetochore, PP2A recruited to BubR1 could facilitate CPC-mediated regulation of kinetochore-proximal MTs (Suijkerbuijk et al., 2012; Kruse et al., 2013; Xu et al., 2013). Given that kinetochore localization of the PP2A B56 subunits are more pronounced in prometaphase than in metaphase (Foley et al., 2011), dephosphorylation of the INCENP PRD may be locally restricted to PP2A-enriched kinetochores during prometaphase. The centromeric PP2A-Sgo1, which inhibits Aurora B activation (Meppelink et al., 2015), may also potentiate MT-dependent activation of Aurora B. It would be interesting to see whether PRD phosphorylation levels change depending on kinetochore attachment status.

The CPC sustains the SAC to promote death in mitosis

Our live-imaging analyses show that the CPC and the INCENP SAH domain sustain the SAC in taxol to promote cell death. We see a strong, linear increase between the median DoM of a sample and the percentage of cells dying in mitosis (Fig. S3 B). The amount of time it took a cell to die in mitosis was similar between all of our constructs, suggesting that the timing of mitotic cell death can be largely uncoupled from the strength of the SAC. This is consistent with the competing-networks model, in which the decision to undergo slippage or death in mitosis is a winner-take-all race between cyclin B degradation and accumulation of pro-apoptotic signals (Gascoigne and Taylor, 2008; Huang et al., 2010; Topham and Taylor, 2013). Our data indicate that even a mild reduction in SAC strength can have a dramatic impact on cell fate during mitotic arrest (Fig. 8).

Materials and methods

Cell culture, siRNA, and drug treatments

HeLa cells were cultured at 37°C with 5% CO_2 in DMEM (Thermo Fisher Scientific) supplemented with 10% tetracycline-free FBS (Atlanta Biologicals) and nonessential amino acids (Thermo Fisher Scientific). HeLa T-Rex cell lines, which stably express the tetracycline repressor, were generated using the manufacturer's protocol from a parental line containing a single FRT integration site and stably integrated RFP-H2B (gift of A. Desai and R. Gassmann, University of California, San Diego, La Jolla, CA; Gassmann et al., 2010).

For live-cell imaging experiments, 300,000 cells were seeded onto glass-bottom dishes (no. 1.5 thickness; MatTek Corporation). After 12–16 h, 100 mg/ml doxycycline was added to induce construct expression, and siRNA was transfected using Lipofectamine RNAiMax (Thermo Fisher Scientific) and 60 pmol of either ON-TARGETplus control siRNA (GE Healthcare) or a previously described siRNA against the coding region of human INCENP (5′-UGACACGGAGAU UGCCAAC-3′; Vader et al., 2006). After 24–36 h, cells were transferred to fresh culture media lacking phenol red before imaging.

For live-cell RO-3306 (RO) synchronization and release experiments (Figs. 4 F and S3 F), cells were plated as described earlier and

allowed to adhere in the presence of doxycycline for 6 h, before the addition of RO for 16–18 h. Cells were rinsed three times in Dulbecco's PBS and placed in fresh media before imaging.

For fixed-cell immunofluorescence, cells were seeded in 10-cm dishes, adhered for 12–16 h, treated with doxycycline and siRNA for 24–36 h, and split onto either poly-D-lysine–coated coverslips or Millicell EZ glass chamber slides (EMD Millipore) and a 6-cm dish (processed in parallel and used to prepare mitotic extracts for immunoblotting). After adhering for 12 h, cells were synchronized with RO for 12 h, followed by three washes in Dulbecco's PBS and addition of fresh media containing either nocodazole or taxol for 2–4 h before fixation. When used, ZM447439 was added 1 h before fixation.

Drug concentrations for human tissue culture cells, unless otherwise indicated, are as follows: 9 µM RO (Sigma-Aldrich), 3.3 µM nocodazole (Sigma-Aldrich), 500 nM taxol (EMD Millipore), 100 µM monastrol (Tocris Bioscience), and 2 µM ZM447439 (Chemietek).

Plasmids

Plasmids are listed in Table S1. All GFP-tagged xINCENP constructs and xSAH domain constructs were prepared from GFP-xINCENP FL (Tseng et al., 2010). FL siRNA-resistant hINCENP was a gift from S. Lens (University Medical Center Utrecht, Utrecht, Netherlands). All human constructs were cloned into a pcDNA5-FRT-TO plasmid containing the LAP tag (gift of R. Gassmann). FL hCENP-B and hCENP-B DNA-binding domain were gifts of M. Lampson (University of Pennsylvania, Philadelphia, PA; Wang et al., 2011). FL hMis12 and a plasmid containing the MAP4-MTBD were gifts of T. Kapoor (Rockefeller University, New York, NY; Maldonado and Kapoor, 2011; Tan and Kapoor, 2011). All human phospho-site mutants were generated using the QuikChange Multi Site-Directed Mutagenesis kit (Agilent Technologies) per the manufacturer's recommendations. *Xenopus* phospho-site mutants were generated using Gibson Assembly (Gibson et al., 2009) with synthesized DNA fragments corresponding to the desired mutations. All constructs either were cloned using QuikChange Site-Directed Mutagenesis (Agilent Technologies), a PCR-based digestion/ligation strategy using a pair of unique restriction sites in the pcDNA5-FRT-TO plasmid, or were generated using Gibson Assembly. The coding frame of all constructs was verified by DNA sequencing before insertion into HeLa T-REx cells.

Immunofluorescence

HeLa cells were fixed in 2% PFA in PBS, pH 7.4, or 1% PFA + 0.2% Triton X-100 (for DSN1 S100ph and KNL1 S24ph [gifts of I. Cheeseman, Massachusetts Institute of Technology, Cambridge, MA] and Hec1 S44ph [gift of J. Deluca, Colorado State University, Fort Collins, CO]) for 10 min at RT (Welburn et al., 2010; DeLuca et al., 2011). Cells were washed once in PBS, permeabilized in PBS + 0.2% Triton X-100 for 10 min, rinsed twice in PBS, and blocked for at least 30 min in 5% BSA + 0.2% Tween 20 (blocking). Cells were incubated in primary antibody diluted in blocking for at least 1 h, rinsed twice in PBS + 0.2% Tween 20 (PBST), and incubated in secondary antibody in blocking for at least 1 h. Cells were rinsed twice in PBST, incubated for at least 5 min in PBS plus 1 µg/ml DAPI, rinsed once in PBS, and mounted with ProLong Gold antifade mountant (Thermo Fisher Scientific). All primary and secondary antibodies are listed in Table S2.

For *Xenopus* egg extract, immunofluorescence of spindles and sperm chromatin was performed as previously published (Desai et al., 1999; Tseng et al., 2010). In brief, extract was diluted in fixative (1× BRB80, 2% formaldehyde) for 5 min, layered over a glycerol cushion, and pelleted onto a stage containing a circular coverslip for 15 min at 51,000 rpm in a Sorvall HS7 swinging-bucket rotor. The cushion was rinsed twice with 1× BRB80 and aspirated away. The coverslip was removed, fixed in ice-cold methanol for 5 min, rinsed twice in 10 mM TBS, pH 7.4, and 0.1% Triton X-100, and incubated with Abdil (10 mM TBS, pH 7.4, 150 mM NaCl, 0.1% Triton X-100, and 2% BSA) overnight at 4°C. Samples were incubated with primary and secondary antibodies diluted in Abdil for at least 1 h, with a 2× PBST rinse after each incubation. Samples were washed once in PBS and mounted with VectaShield antifade mountant containing DAPI (Vector Laboratories).

Live cell imaging and analysis

Live cell imaging was performed at 37°C in 5% CO_2 in a LCV110U VivaView FL incubator microscope (Olympus) equipped with an X-Cite-exacte illumination source (Excelitas Technologies) and Orca-R2 CCD camera (Hamamatsu Photonics). For SAC experiments, spindle poisons diluted in media were added to each dish at least 20 min before imaging. For RO synchronization and release experiments, samples were imaged directly after the final washout. For taxol and RO synchronization and release experiments, images were acquired with a 20× objective every 15 min for 48–72 h in the differential interference contrast (DIC), RFP, and GFP channels. For enhanced time resolution of unperturbed mitosis (Fig. 7 F), cells were imaged every 5 min. Individual cells were manually analyzed using the CellCognition browser. DoM and class at exit from mitosis were inferred from DIC and RFP morphology (Fig. S3 A). For SAC experiments, only cells observed transitioning from interphase to mitosis during the first 16 h of the video were analyzed. The DoM was calculated as the time from NEB until either slippage into interphase or cell death.

For RO synchronization and release experiments (Figs. 4 F and S3 F), each sample was imaged before washout to verify that >95% of cells were in interphase. After washout, cells in prophase/prometaphase at the beginning of the video or those seen transitioning into mitosis within the first 6 h of the video were analyzed. The DoM was calculated as the time from NEB until chromosome segregation or cell death.

Image acquisition and processing

Immunofluorescence images were acquired on a DeltaVision Image Restoration Microscope (Applied Precision Ltd.) using an inverted IX-70 stage (Olympus), pco.edge sCOS camera (PCO), Insight SSI solid-state illumination system (Applied Precision Ltd.), and 20×/0.75 air and 100×/1.4 oil objectives (Olympus) and running SoftWoRx v6.1 software (Applied Precision Ltd.). Images were acquired at RT using immersion oil with a refractory index of 1.516. The fluorophores DAPI, Dylight594, Alexa Fluor 488, and Cy5 were detected using filters for DAPI, Alexa Fluor 594, FITC, and Cy5, respectively. All images were acquired as *z*-stacks with 0.4-µm optical sectioning and deconvolved using SoftWoRx constrained iterative deconvolution with default settings. All images within an experiment used identical acquisition settings.

For image quantification, deconvolved stacks were exported as 16-bit TIFFS and quantified using MetaMorph (Molecular Devices). For each sample, a maximum projection of the DAPI channel was used to create a DAPI region to select a single cell within a field. Epitopes that form foci at the centromere or kinetochore have the highest intensity in these regions; therefore, we empirically determined a threshold that primarily captured these intense foci, while excluding the signal outside these regions. This threshold was applied to each plane of the *z*-stack to quantify the integrated intensity of foci for the epitope. In a single experiment, each sample was quantified using the same threshold for a given channel. Images for which this threshold did not capture primarily centromere/kinetochore signal (for example, because of an artifact or high background) were discarded. A mean of ∼10% or fewer cells from each sample were discarded for this reason.

Kinetochore intensity for phospho-specific kinetochore antibodies (Dsn1 S100ph, Knl1 S24ph) was quantified using a marker channel,

stained by anti–CENP-C antibody (a gift of H. Kimura, Tokyo Institute of Technology, Tokyo, Japan; Ando et al., 2002), to manually place a circle of defined size around each kinetochore. These kinetochore regions were then used to quantify the signal intensity from a maximum projection of the phospho-specific antibody channel. To calculate individual kinetochore intensity for Hec1 S44ph relative to Hec1, a threshold/watershed segmentation was performed on the Hec1 channel to create kinetochore regions. These regions were then used to quantify the intensity of Hec1 and Hec1 S44ph at each kinetochore from a maximum projection of each channel.

Automated foci counts were performed using MetaMorph. A mask generated from the DAPI channel was used to select a single cell within a field. For the channel of interest, a threshold/watershed segmentation was performed to separate individual foci. All foci larger than a minimum size were counted for each cell, yielding the number of foci per cell for a given epitope. The segmented regions were manually inspected for a subset of the total images.

Immunoblotting

Mitotic HeLa cell extracts were prepared by placing cells in 0.33 µM nocodazole for 6–8 h followed by mitotic shake-off. Cells were pelleted at 200 *g*, rinsed twice in PBS, and resuspended in 2× Laemmli buffer. Extracts were sonicated at 4°C in a Bioruptor water bath (Diagenode) at medium-intensity cycling 30 s on/60 s off for a total of 10 min. Samples were denatured, the protein concentration was determined using 260/280 nm on a NanoDrop 2000, and an equal amount of each sample was run on a precast 4–12% Bis-Tris gel (Thermo Fisher Scientific) followed by transfer to a nitrocellulose membrane overnight at 30 V. For *Xenopus* egg extract, samples were diluted in sample buffer, denatured, run on a precast gel as described earlier, and transferred to a nitrocellulose membrane overnight at 15 V.

Membranes were blocked in sterile 4% nonfat milk in PBS for at least 30 min, followed by incubation with primary antibody diluted in 5% BSA for 1–6 h at RT. After three 5-min washes in PBST, the membranes were incubated for 1 h with IRDye 800CW and 680LT secondary antibodies diluted in Odyssey Blocking Buffer with 0.1% Tween. Membranes were then washed three times for 5 min in PBST and detected using the Odyssey Infrared Imaging System (LI-COR Biosciences). All antibody information is listed in Table S2. Anti-NuMA antibody was a gift of R. Heald (University of California, Berkeley, Berkeley, CA).

FRAP

After 36- to 48-h siRNA treatment and construct induction, cells were treated with 3.3 µM nocodazole or 500 nM taxol for 1 h then placed in a 37°C chamber mounted on a Deltavision Image Restoration System microscope (see Image acquisition and processing). FRAP was performed using SoftWoRx v6.1 software and a 488-nm QLM laser pulse to bleach three centromeric foci per cell. Images were acquired with a 60×/1.42 oil objective from a single *z*-section every 10 s for 30 s before and 5 min after bleaching. Quantification was performed in ImageJ using a circle of defined size to quantify the integrated intensity of each bleached focus, a same-sized background focus, and the entire cell. Only foci remaining in the focal plane for the duration of the video were quantified. Full-scale normalization and single-exponential fitting were performed in Matlab using the easyFRAP module (Rapsomaniki et al., 2012) to determine the $t_{1/2}$ of each focus.

Immunoprecipitation

For immunoprecipitation from mitotic HeLa cell extracts, construct expression was induced by doxycycline in a confluent 15-cm dish for 8 h followed by the addition of 100 ng/ml nocodazole for 16 h. Mitotic cells were collected by shake-off, rinsed in 1× PBS, resuspended in 50 µl of 1× PBS, and incubated in lysis buffer (50 mM Tris, pH 8, 150 mM NaCl, 1% NP-40, 0.5 mM PMSF, 5 mM β-glycerol phosphate, phosphatase inhibitor cocktail [Roche)], and EDTA-free protease inhibitor [Sigma-Aldrich]) for 30 min. Samples were sonicated in a water bath 5× 10 s on/10 s off and passaged through a 251/4 gauge needle. Samples were clarified by spinning for 10 min at maximum speed in a tabletop centrifuge. Clarified lysate was incubated with magnetic beads cross-linked to rabbit IgG or rabbit anti-GFP antibodies for 1.5 h with constant agitation. Beads were removed, rinsed once in lysis buffer, resuspended in sample buffer, and boiled. Half the sample was loaded for Western blot analysis. All steps were performed at 4°C.

Xenopus egg extract

A published protocol was used to prepare CSF extracts (Murray, 1991). Depletion of endogenous CPC and reconstitution was previously described (Tseng et al., 2010). For depletion, magnetic protein A Dynabeads (Invitrogen) were coupled and cross-linked to either rabbit anti-IgG or rabbit anti-xINCENP beads using BS_3 (Thermo Fisher Scientific) according to the manufacturer's recommendations. CSF extract was incubated with the appropriate beads in a 1:1 ratio for 1 h at 4°C, then beads were removed to yield depleted extract. The CPC was reconstituted in ΔCPC extract by the addition of 500 nM recombinant MBP-xAurora B, 0.3 µg/µl of mRNA for the appropriate GFP-xINCENP construct, and 0.075 µg/µl each of mRNA encoding xSurvivin and xDasra A. To translate these mRNA constructs, extract was cycled into interphase by the addition of 300 µM calcium chloride for 1.5 h at 22°C, then driven back into metaphase by adding an equal volume of fresh CSF extract and incubating for 30–45 min at 22°C. mRNA was prepared using the SP6 mMessage mMachine RNA transcription kit (Ambion). All xSAH domain fragments were expressed from mRNA added to extract at 0.15–0.3 µg/µl and cycled as described earlier. Immunoprecipitation of GFP and GFP-xSAH was performed similarly to CPC depletion using rabbit anti-GFP antibodies.

For immunofluorescence on nocodazole-treated sperm chromatin, 1,000–2,000 sperm/µl were added before calcium addition. After incubation with fresh CSF, samples were incubated with 33 µM nocodazole for 30 min before processing for immunofluorescence.

The SAC assay was performed similarly to Minshull et al. (1994). In brief, samples were reconstituted as described earlier. CSF extract was then incubated with 10,000 sperm/µl and 33 µM nocodazole for 45 min, followed by addition of 600 µM calcium chloride. Western blot samples were taken at 30-min intervals after the addition of calcium chloride.

MT pelleting assays were modified from Xue et al. (2013). Extract was incubated for 30 min with 33 µM nocodazole or 10 µM taxol at 22°C. An input sample was taken, and 20 µl of extract was diluted in fixative (1× BRB80, 30% glycerol, 0.1% Triton X-100, and phosphatase inhibitor) and layered over a glycerol cushion (1× BRB80 and 40% glycerol). Samples were spun in a tabletop centrifuge at RT for 15 min at maximum speed. The cushion was washed twice with 1× BRB80 and aspirated away, and the pellet was resuspended in 1× BRB80 and 0.1% Triton X-100 and transferred to a fresh tube. The sample was spun again for 15 min, and the pellet was resuspended in 40 µl sample buffer. For phosphatase treatment, samples were diluted in buffer containing lambda phosphatase for 40 min at 30°C (New England Biolabs, Inc.).

CENP-A nucleosome arrays were assembled according to Guse et al. (2011). In brief, chromatin was assembled by salt dialysis of 3.6 µM human CENP-A/*Xenopus* H4 dimers that had been co-purified from bacteria using hydroxyapatite (Bio-Rad Laboratories) and HiTrap SP (GE Healthcare) columns, 4.0 µM *Xenopus* H2A/H2B dimers generated by purifying his-tagged constructs separately from

inclusion bodies using Ni-NTA (QIAGEN) and dialyzed together after cleavage of the His tags using TEV protease (Zierhut et al., 2014), and 0.2 µg/µl of a DNA fragment containing 19 copies of the 601 nucleosome positioning sequence, which had been biotinylated on both ends using Klenow (New England Biolabs, Inc.) in the presence of biotin-14-dATP, thio-dTTP, and thio-dGTP. Plasmids encoding this DNA template and for CENP-A/H4 coexpression were gifts from A. Straight (Stanford University, Stanford, CA). Plasmids for expression of His-H2A and His-H2B were gifts from C.D. Allis (Rockefeller University, New York, NY). Coupling to Dynabeads M-280 Streptavidin (Thermo Fisher Scientific) at a concentration in which 1 µg of DNA was coupled to 10 µl of bead slurry for 1 h was done just before addition to extract. To assay CPC localization, array-coupled beads were added to a final volume of 100 µl control (ΔIgG), CPC-depleted, or CPC-reconstituted extract. Extracts were then cycled to express RNA, and 33 µM nocodazole was added. Beads were removed from extract with a magnet, washed in ice-cold CSF-XB with 0.05% Triton X-100, fixed for 5 min in 2% formaldehyde, washed with Abdil, added to acid-washed, poly-L-lysine–coated coverslips, and processed for immunofluorescence in the same manner as sperm chromosomes.

Data presentation

Broken violin plots were generated using a custom script in Python 2.7. In brief, a kernel density estimate of the underlying data was determined using the scipy.stats.gaussian_kde module with a bandwidth determined by the Scott method. The integrated area underneath each density estimate is equal between all samples in a plot unless otherwise indicated. For visualization, density estimates were cut at the minimum and maximum value of the underlying data. Beneath each density is a minimalist boxplot with a lower whisker from −1.5 × IQR to the first quartile, a circle at the median, and an upper whisker from the third quartile to 1.5 × IQR. Data were organized using the Pandas module, programmatically visualized using matplotlib and seaborn modules, and labeled and formatted in Adobe Illustrator CC.

Representative images are no more than ±20% of the median value of the construct based on quantification. Representative images from qualitative experiments were chosen based on morphology. Graphs were generated using Python or Prism software. All box plots are Tukey box plots with whiskers extending ±1.5 × IQR. For visual simplicity, points past the whiskers (considered statistical outliers) are omitted. All statistical analyses were conducted in Prism using a two-tailed Mann–Whitney test using all samples (even statistical outliers). Individual p-values and *n* values are indicated in figure legends. In several cases, data from multiple independent experiments were aggregated and used for statistics. Aggregation was performed by normalizing the intensity of each sample to hINCENP FL within that experiment, then pooling these normalized values from multiple experiments together. For these experiments, representative images were chosen from a single experiment.

Online supplemental material

Fig. S1 shows characterization of 6Myc-xSAH in *Xenopus* egg extracts. Fig. S2 shows CPC binding and localization analyses of GFP-INCENP ΔSAH in HeLa cells. Fig. S3 (A and B) shows mitotic fates upon taxol treatment, Fig. S3 (C–E) shows immunofluorescence of kinetochore markers in HeLa cells whose INCENP was replaced with INCENP SAH deletion mutants, and Fig. S3 F shows a control for Fig. 4 F. Fig. S4 A shows immunofluorescence of 6My-tagged xINCENP SAH domain constructs in *Xenopus* egg extracts, and Fig. S4 B shows sequence alignment of PRD1 and PRD2. Fig. S5 A shows the effect of C-terminal deletion of the SAH on DoM in taxol-treated HeLa cells, and Fig. S5 B shows the effect of expressing INCENP 6A on unperturbed HeLa cells. Tables S1 and S2 list plasmids and antibodies used in this study, respectively.

Acknowledgments

We thank I. Cheeseman, J. Deluca, A. Desai, R. Gassmann, R. Heald, T. Kapoor, H. Kimura, M. Lampson, S. Lens, and A. Straight for reagents. We thank C. Sommer and D. Gerlich for development of the CellCognition Browser.

D.S. Wheelock was supported by a National Research Service Award postdoctoral fellowship (F32GM103147). B.S. Tseng and M.S. Wheelock were supported by the National Institutes of Health (T32GM066699). This work was supported by a grant from National Institutes of Health to H. Funabiki (R01GM075249) and to the Bio-Imaging Resource Center (S10RR031855). The content is solely the responsibility of the authors and does not necessarily represent the official views of the National Institutes of Health.

The authors declare no competing financial interests.

Author contributions: M.S. Wheelock designed and executed all experiments and analyzed data, except for an experiment shown in Fig. 1C, which was performed by D.J. Wynne. D.J. Wynne and B.S. Tseng have generated preliminary data in *Xenopus* egg extracts, which guided this study. H. Funabiki supervised the entire study. M.S. Wheelock and H. Funabiki wrote the manuscript, which was edited by D.J. Wynne and B.S. Tseng.

Submitted: 13 September 2016
Revised: 11 January 2017
Accepted: 7 February 2017

References

Adams, R.R., S.P. Wheatley, A.M. Gouldsworthy, S.E. Kandels-Lewis, M. Carmena, C. Smythe, D.L. Gerloff, and W.C. Earnshaw. 2000. INC ENP binds the Aurora-related kinase AIRK2 and is required to target it to chromosomes, the central spindle and cleavage furrow. *Curr. Biol.* 10:1075–1078. http://dx.doi.org/10.1016/S0960-9822(00)00673-4

Akiyoshi, B., K.K. Sarangapani, A.F. Powers, C.R. Nelson, S.L. Reichow, H. Arellano-Santoyo, T. Gonen, J.A. Ranish, C.L. Asbury, and S. Biggins. 2010. Tension directly stabilizes reconstituted kinetochore-microtubule attachments. *Nature.* 468:576–579. http://dx.doi.org/10.1038/nature09594

Akiyoshi, B., C.R. Nelson, and S. Biggins. 2013. The aurora B kinase promotes inner and outer kinetochore interactions in budding yeast. *Genetics.* 194:785–789. http://dx.doi.org/10.1534/genetics.113.150839

Alexander, J., D. Lim, B.A. Joughin, B. Hegemann, J.R. Hutchins, T. Ehrenberger, F. Ivins, F. Sessa, O. Hudecz, E.A. Nigg, et al. 2011. Spatial exclusivity combined with positive and negative selection of phosphorylation motifs is the basis for context-dependent mitotic signaling. *Sci. Signal.* 4:ra42. http://dx.doi.org/10.1126/scisignal.2001796

Alushin, G.M., V.H. Ramey, S. Pasqualato, D.A. Ball, N. Grigorieff, A. Musacchio, and E. Nogales. 2010. The Ndc80 kinetochore complex forms oligomeric arrays along microtubules. *Nature.* 467:805–810. http://dx.doi.org/10.1038/nature09423

Ando, S., H. Yang, N. Nozaki, T. Okazaki, and K. Yoda. 2002. CENP-A, -B, and -C chromatin complex that contains the I-type alpha-satellite array constitutes the prekinetochore in HeLa cells. *Mol. Cell. Biol.* 22:2229–2241. http://dx.doi.org/10.1128/MCB.22.7.2229-2241.2002

Banerjee, B., C.A. Kestner, and P.T. Stukenberg. 2014. EB1 enables spindle microtubules to regulate centromeric recruitment of Aurora B. *J. Cell Biol.* 204:947–963. http://dx.doi.org/10.1083/jcb.201307119

Bekier, M.E., T. Mazur, M.S. Rashid, and W.R. Taylor. 2015. Borealin dimerization mediates optimal CPC checkpoint function by enhancing localization to centromeres and kinetochores. *Nat. Commun.* 6:6775. http://dx.doi.org/10.1038/ncomms7775

Bishop, J.D., and J.M. Schumacher. 2002. Phosphorylation of the carboxyl terminus of inner centromere protein (INCENP) by the Aurora B kinase stimulates Aurora B kinase activity. *J. Biol. Chem.* 277:27577–27580. http://dx.doi.org/10.1074/jbc.C200307200

Bourhis, E., A. Lingel, Q. Phung, W.J. Fairbrother, and A.G. Cochran. 2009. Phosphorylation of a borealin dimerization domain is required for proper chromosome segregation. *Biochemistry.* 48:6783–6793. http://dx.doi.org/10.1021/bi900530v

Campbell, C.S., and A. Desai. 2013. Tension sensing by Aurora B kinase is independent of survivin-based centromere localization. *Nature.* 497:118–121. http://dx.doi.org/10.1038/nature12057

Carmena, M., M. Wheelock, H. Funabiki, and W.C. Earnshaw. 2012. The chromosomal passenger complex (CPC): From easy rider to the godfather of mitosis. *Nat. Rev. Mol. Cell Biol.* 13:789–803. http://dx.doi.org/10.1038/nrm3474

Chan, Y.W., A.A. Jeyaprakash, E.A. Nigg, and A. Santamaria. 2012. Aurora B controls kinetochore-microtubule attachments by inhibiting Ska complex-KMN network interaction. *J. Cell Biol.* 196:563–571. http://dx.doi.org/10.1083/jcb.201109001

Cheeseman, I.M., and A. Desai. 2005. A combined approach for the localization and tandem affinity purification of protein complexes from metazoans. *Sci. STKE.* 2005:pl1.

Cheng, L., J. Zhang, S. Ahmad, L. Rozier, H. Yu, H. Deng, and Y. Mao. 2011. Aurora B regulates formin mDia3 in achieving metaphase chromosome alignment. *Dev. Cell.* 20:342–352. http://dx.doi.org/10.1016/j.devcel.2011.01.008

DeLuca, J.G., W.E. Gall, C. Ciferri, D. Cimini, A. Musacchio, and E.D. Salmon. 2006. Kinetochore microtubule dynamics and attachment stability are regulated by Hec1. *Cell.* 127:969–982. http://dx.doi.org/10.1016/j.cell.2006.09.047

DeLuca, K.F., S.M. Lens, and J.G. DeLuca. 2011. Temporal changes in Hec1 phosphorylation control kinetochore-microtubule attachment stability during mitosis. *J. Cell Sci.* 124:622–634. http://dx.doi.org/10.1242/jcs.072629

Desai, A., A. Murray, T.J. Mitchison, and C.E. Walczak. 1999. The use of *Xenopus* egg extracts to study mitotic spindle assembly and function in vitro. *Methods Cell Biol.* 61:385–412. http://dx.doi.org/10.1016/S0091-679X(08)61991-3

Ditchfield, C., V.L. Johnson, A. Tighe, R. Ellston, C. Haworth, T. Johnson, A. Mortlock, N. Keen, and S.S. Taylor. 2003. Aurora B couples chromosome alignment with anaphase by targeting BubR1, Mad2, and Cenp-E to kinetochores. *J. Cell Biol.* 161:267–280. http://dx.doi.org/10.1083/jcb.200208091

Etemad, B., T.E. Kuijt, and G.J. Kops. 2015. Kinetochore-microtubule attachment is sufficient to satisfy the human spindle assembly checkpoint. *Nat. Commun.* 6:8987. http://dx.doi.org/10.1038/ncomms9987

Foley, E.A., and T.M. Kapoor. 2013. Microtubule attachment and spindle assembly checkpoint signalling at the kinetochore. *Nat. Rev. Mol. Cell Biol.* 14:25–37. http://dx.doi.org/10.1038/nrm3494

Foley, E.A., M. Maldonado, and T.M. Kapoor. 2011. Formation of stable attachments between kinetochores and microtubules depends on the B56-PP2A phosphatase. *Nat. Cell Biol.* 13:1265–1271. http://dx.doi.org/10.1038/ncb2327

Gadea, B.B., and J.V. Ruderman. 2005. Aurora kinase inhibitor ZM447439 blocks chromosome-induced spindle assembly, the completion of chromosome condensation, and the establishment of the spindle integrity checkpoint in *Xenopus* egg extracts. *Mol. Biol. Cell.* 16:1305–1318. http://dx.doi.org/10.1091/mbc.E04-10-0891

Gascoigne, K.E., and S.S. Taylor. 2008. Cancer cells display profound intra- and interline variation following prolonged exposure to antimitotic drugs. *Cancer Cell.* 14:111–122. http://dx.doi.org/10.1016/j.ccr.2008.07.002

Gassmann, R., A. Carvalho, A.J. Henzing, S. Ruchaud, D.F. Hudson, R. Honda, E.A. Nigg, D.L. Gerloff, and W.C. Earnshaw. 2004. Borealin: A novel chromosomal passenger required for stability of the bipolar mitotic spindle. *J. Cell Biol.* 166:179–191. http://dx.doi.org/10.1083/jcb.200404001

Gassmann, R., A.J. Holland, D. Varma, X. Wan, F. Civril, D.W. Cleveland, K. Oegema, E.D. Salmon, and A. Desai. 2010. Removal of Spindly from microtubule-attached kinetochores controls spindle checkpoint silencing in human cells. *Genes Dev.* 24:957–971. http://dx.doi.org/10.1101/gad.1886810

Gibson, D.G., L. Young, R.Y. Chuang, J.C. Venter, C.A. Hutchison III, and H.O. Smith. 2009. Enzymatic assembly of DNA molecules up to several hundred kilobases. *Nat. Methods.* 6:343–345. http://dx.doi.org/10.1038/nmeth.1318

Guse, A., C.W. Carroll, B. Moree, C.J. Fuller, and A.F. Straight. 2011. In vitro centromere and kinetochore assembly on defined chromatin templates. *Nature.* 477:354–358. http://dx.doi.org/10.1038/nature10379

Hauf, S., R.W. Cole, S. LaTerra, C. Zimmer, G. Schnapp, R. Walter, A. Heckel, J. van Meel, C.L. Rieder, and J.M. Peters. 2003. The small molecule Hesperadin reveals a role for Aurora B in correcting kinetochore-microtubule attachment and in maintaining the spindle assembly checkpoint. *J. Cell Biol.* 161:281–294. http://dx.doi.org/10.1083/jcb.200208092

Honda, R., R. Körner, and E.A. Nigg. 2003. Exploring the functional interactions between Aurora B, INCENP, and survivin in mitosis. *Mol. Biol. Cell.* 14:3325–3341. http://dx.doi.org/10.1091/mbc.E02-11-0769

Hsu, J.Y., Z.W. Sun, X. Li, M. Reuben, K. Tatchell, D.K. Bishop, J.M. Grushcow, C.J. Brame, J.A. Caldwell, D.F. Hunt, et al. 2000. Mitotic phosphorylation of histone H3 is governed by Ipl1/aurora kinase and Glc7/PP1 phosphatase in budding yeast and nematodes. *Cell.* 102:279–291. http://dx.doi.org/10.1016/S0092-8674(00)00034-9

Huang, H.C., T.J. Mitchison, and J. Shi. 2010. Stochastic competition between mechanistically independent slippage and death pathways determines cell fate during mitotic arrest. *PLoS One.* 5:e15724. http://dx.doi.org/10.1371/journal.pone.0015724

Hümmer, S., and T.U. Mayer. 2009. Cdk1 negatively regulates midzone localization of the mitotic kinesin Mklp2 and the chromosomal passenger complex. *Curr. Biol.* 19:607–612. http://dx.doi.org/10.1016/j.cub.2009.02.046

Iimori, M., S. Watanabe, S. Kiyonari, K. Matsuoka, R. Sakasai, H. Saeki, E. Oki, H. Kitao, and Y. Maehara. 2016. Phosphorylation of EB2 by Aurora B and CDK1 ensures mitotic progression and genome stability. *Nat. Commun.* 7:11117. http://dx.doi.org/10.1038/ncomms11117

Jeyaprakash, A.A., U.R. Klein, D. Lindner, J. Ebert, E.A. Nigg, and E. Conti. 2007. Structure of a Survivin-Borealin-INCENP core complex reveals how chromosomal passengers travel together. *Cell.* 131:271–285. http://dx.doi.org/10.1016/j.cell.2007.07.045

Kallio, M.J., M.L. McCleland, P.T. Stukenberg, and G.J. Gorbsky. 2002. Inhibition of aurora B kinase blocks chromosome segregation, overrides the spindle checkpoint, and perturbs microtubule dynamics in mitosis. *Curr. Biol.* 12:900–905. http://dx.doi.org/10.1016/S0960-9822(02)00887-4

Kapoor, T.M., T.U. Mayer, M.L. Coughlin, and T.J. Mitchison. 2000. Probing spindle assembly mechanisms with monastrol, a small molecule inhibitor of the mitotic kinesin, Eg5. *J. Cell Biol.* 150:975–988. http://dx.doi.org/10.1083/jcb.150.5.975

Kapoor, T.M., M.A. Lampson, P. Hergert, L. Cameron, D. Cimini, E.D. Salmon, B.F. McEwen, and A. Khodjakov. 2006. Chromosomes can congress to the metaphase plate before biorientation. *Science.* 311:388–391. http://dx.doi.org/10.1126/science.1122142

Kelly, A.E., S.C. Sampath, T.A. Maniar, E.M. Woo, B.T. Chait, and H. Funabiki. 2007. Chromosomal enrichment and activation of the aurora B pathway are coupled to spatially regulate spindle assembly. *Dev. Cell.* 12:31–43. http://dx.doi.org/10.1016/j.devcel.2006.11.001

Kelly, A.E., C. Ghenoiu, J.Z. Xue, C. Zierhut, H. Kimura, and H. Funabiki. 2010. Survivin reads phosphorylated histone H3 threonine 3 to activate the mitotic kinase Aurora B. *Science.* 330:235–239. http://dx.doi.org/10.1126/science.1189505

Kim, S., and H. Yu. 2015. Multiple assembly mechanisms anchor the KMN spindle checkpoint platform at human mitotic kinetochores. *J. Cell Biol.* 208:181–196. http://dx.doi.org/10.1083/jcb.201407074

Klein, U.R., E.A. Nigg, and U. Gruneberg. 2006. Centromere targeting of the chromosomal passenger complex requires a ternary subcomplex of Borealin, Survivin, and the N-terminal domain of INCENP. *Mol. Biol. Cell.* 17:2547–2558. http://dx.doi.org/10.1091/mbc.E05-12-1133

Knowlton, A.L., W. Lan, and P.T. Stukenberg. 2006. Aurora B is enriched at merotelic attachment sites, where it regulates MCAK. *Curr. Biol.* 16:1705–1710. http://dx.doi.org/10.1016/j.cub.2006.07.057

Krupina, K., C. Kleiss, T. Metzger, S. Fournane, S. Schmucker, K. Hofmann, B. Fischer, N. Paul, I.M. Porter, W. Raffelsberger, et al. 2016. Ubiquitin receptor protein UBASH3B drives Aurora B recruitment to mitotic microtubules. *Dev. Cell.* 36:63–78. http://dx.doi.org/10.1016/j.devcel.2015.12.017

Kruse, T., G. Zhang, M.S. Larsen, T. Lischetti, W. Streicher, T. Kragh Nielsen, S.P. Bjørn, and J. Nilsson. 2013. Direct binding between BubR1 and B56-PP2A phosphatase complexes regulate mitotic progression. *J. Cell Sci.* 126:1086–1092. http://dx.doi.org/10.1242/jcs.122481

Landau, M., I. Mayrose, Y. Rosenberg, F. Glaser, E. Martz, T. Pupko, and N. Ben-Tal. 2005. ConSurf 2005: The projection of evolutionary conservation scores of residues on protein structures. *Nucleic Acids Res.* 33(suppl 2):W299–W302. http://dx.doi.org/10.1093/nar/gki370

Lens, S.M., J.A. Rodriguez, G. Vader, S.W. Span, G. Giaccone, and R.H. Medema. 2006. Uncoupling the central spindle-associated function of the chromosomal passenger complex from its role at centromeres. *Mol. Biol. Cell.* 17:1897–1909. http://dx.doi.org/10.1091/mbc.E05-08-0727

Liu, D., G. Vader, M.J.M. Vromans, M.A. Lampson, and S.M.A. Lens. 2009. Sensing chromosome bi-orientation by spatial separation of aurora B kinase from kinetochore substrates. *Science.* 323:1350–1353. http://dx.doi.org/10.1126/science.1167000

Liu, D., M. Vleugel, C.B. Backer, T. Hori, T. Fukagawa, I.M. Cheeseman, and M.A. Lampson. 2010. Regulated targeting of protein phosphatase 1 to the outer kinetochore by KNL1 opposes Aurora B kinase. *J. Cell Biol.* 188:809–820. http://dx.doi.org/10.1083/jcb.201001006

London, N., and S. Biggins. 2014. Mad1 kinetochore recruitment by Mps1-mediated phosphorylation of Bub1 signals the spindle checkpoint. *Genes Dev.* 28:140–152. http://dx.doi.org/10.1101/gad.233700.113

London, N., S. Ceto, J.A. Ranish, and S. Biggins. 2012. Phosphoregulation of Spc105 by Mps1 and PP1 regulates Bub1 localization to kinetochores. *Curr. Biol.* 22:900–906. http://dx.doi.org/10.1016/j.cub.2012.03.052

Mackay, A.M., D.M. Eckley, C. Chue, and W.C. Earnshaw. 1993. Molecular analysis of the INCENPs (inner centromere proteins): Separate domains are required for association with microtubules during interphase and with the central spindle during anaphase. *J. Cell Biol.* 123:373–385. http://dx.doi.org/10.1083/jcb.123.2.373

Makrantoni, V., S.J. Corbishley, N. Rachidi, N.A. Morrice, D.A. Robinson, and M.J. Stark. 2014. Phosphorylation of Sli15 by Ipl1 is important for proper CPC localization and chromosome stability in *Saccharomyces cerevisiae*. *PLoS One.* 9:e89399. http://dx.doi.org/10.1371/journal.pone.0089399

Maldonado, M., and T.M. Kapoor. 2011. Constitutive Mad1 targeting to kinetochores uncouples checkpoint signalling from chromosome biorientation. *Nat. Cell Biol.* 13:475–482. http://dx.doi.org/10.1038/ncb2223

Meppelink, A., L. Kabeche, M.J. Vromans, D.A. Compton, and S.M. Lens. 2015. Shugoshin-1 balances Aurora B kinase activity via PP2A to promote chromosome bi-orientation. *Cell Reports.* 11:508–515. http://dx.doi.org/10.1016/j.celrep.2015.03.052

Minshull, J., H. Sun, N.K. Tonks, and A.W. Murray. 1994. A MAP-kinase dependent spindle assembly checkpoint in *Xenopus* egg extracts. *Cell.* 79:475–486. http://dx.doi.org/10.1016/0092-8674(94)90256-9

Mirchenko, L., and F. Uhlmann. 2010. Sli15(INCENP) dephosphorylation prevents mitotic checkpoint reengagement due to loss of tension at anaphase onset. *Curr. Biol.* 20:1396–1401. http://dx.doi.org/10.1016/j.cub.2010.06.023

Murray, A.W. 1991. Cell cycle extracts. *Methods Cell Biol.* 36:581–605. http://dx.doi.org/10.1016/S0091-679X(08)60298-8

Nijenhuis, W., E. von Castelmur, D. Littler, V. De Marco, E. Tromer, M. Vleugel, M.H. van Osch, B. Snel, A. Perrakis, and G.J. Kops. 2013. A TPR domain-containing N-terminal module of MPS1 is required for its kinetochore localization by Aurora B. *J. Cell Biol.* 201:217–231. http://dx.doi.org/10.1083/jcb.201210033

Pereira, G., and E. Schiebel. 2003. Separase regulates INCENP-Aurora B anaphase spindle function through Cdc14. *Science.* 302:2120–2124. http://dx.doi.org/10.1126/science.1091936

Primorac, I., J.R. Weir, E. Chiroli, F. Gross, I. Hoffmann, S. van Gerwen, A. Ciliberto, and A. Musacchio. 2013. Bub3 reads phosphorylated MELT repeats to promote spindle assembly checkpoint signaling. *eLife.* 2:e01030. http://dx.doi.org/10.7554/eLife.01030

Rapsomaniki, M.A., P. Kotsantis, I.E. Symeonidou, N.N. Giakoumakis, S. Taraviras, and Z. Lygerou. 2012. easyFRAP: An interactive, easy-to-use tool for qualitative and quantitative analysis of FRAP data. *Bioinformatics.* 28:1800–1801. http://dx.doi.org/10.1093/bioinformatics/bts241

Rosenberg, J.S., F.R. Cross, and H. Funabiki. 2011. KNL1/Spc105 recruits PP1 to silence the spindle assembly checkpoint. *Curr. Biol.* 21:942–947. http://dx.doi.org/10.1016/j.cub.2011.04.011

Samejima, K., M. Platani, M. Wolny, H. Ogawa, G. Vargiu, P.J. Knight, M. Peckham, and W.C. Earnshaw. 2015. The inner centromere protein (INCENP) coil is a single α-helix (SAH) domain that binds directly to microtubules and is important for chromosome passenger complex (CPC) localization and function in mitosis. *J. Biol. Chem.* 290:21460–21472. http://dx.doi.org/10.1074/jbc.M115.645317

Sampath, S.C., R. Ohi, O. Leismann, A. Salic, A. Pozniakovski, and H. Funabiki. 2004. The chromosomal passenger complex is required for chromatin-induced microtubule stabilization and spindle assembly. *Cell.* 118:187–202. http://dx.doi.org/10.1016/j.cell.2004.06.026

Santaguida, S., C. Vernieri, F. Villa, A. Ciliberto, and A. Musacchio. 2011. Evidence that Aurora B is implicated in spindle checkpoint signalling independently of error correction. *EMBO J.* 30:1508–1519. http://dx.doi.org/10.1038/emboj.2011.70

Saurin, A.T., M.S. van der Waal, R.H. Medema, S.M. Lens, and G.J. Kops. 2011. Aurora B potentiates Mps1 activation to ensure rapid checkpoint establishment at the onset of mitosis. *Nat. Commun.* 2:316. http://dx.doi.org/10.1038/ncomms1319

Sessa, F., M. Mapelli, C. Ciferri, C. Tarricone, L.B. Areces, T.R. Schneider, P.T. Stukenberg, and A. Musacchio. 2005. Mechanism of Aurora B activation by INCENP and inhibition by hesperadin. *Mol. Cell.* 18:379–391. http://dx.doi.org/10.1016/j.molcel.2005.03.031

Shepperd, L.A., J.C. Meadows, A.M. Sochaj, T.C. Lancaster, J. Zou, G.J. Buttrick, J. Rappsilber, K.G. Hardwick, and J.B. Millar. 2012. Phosphodependent recruitment of Bub1 and Bub3 to Spc7/KNL1 by Mph1 kinase maintains the spindle checkpoint. *Curr. Biol.* 22:891–899. http://dx.doi.org/10.1016/j.cub.2012.03.051

Suijkerbuijk, S.J., M. Vleugel, A. Teixeira, and G.J. Kops. 2012. Integration of kinase and phosphatase activities by BUBR1 ensures formation of stable kinetochore-microtubule attachments. *Dev. Cell.* 23:745–755. http://dx.doi.org/10.1016/j.devcel.2012.09.005

Tan, L., and T.M. Kapoor. 2011. Examining the dynamics of chromosomal passenger complex (CPC)-dependent phosphorylation during cell division. *Proc. Natl. Acad. Sci. USA.* 108:16675–16680. http://dx.doi.org/10.1073/pnas.1106748108

Tauchman, E.C., F.J. Boehm, and J.G. DeLuca. 2015. Stable kinetochore-microtubule attachment is sufficient to silence the spindle assembly checkpoint in human cells. *Nat. Commun.* 6:10036. http://dx.doi.org/10.1038/ncomms10036

Tipton, A.R., W. Ji, B. Sturt-Gillespie, M.E. Bekier II, K. Wang, W.R. Taylor, and S.T. Liu. 2013. Monopolar spindle 1 (MPS1) kinase promotes production of closed MAD2 (C-MAD2) conformer and assembly of the mitotic checkpoint complex. *J. Biol. Chem.* 288:35149–35158. http://dx.doi.org/10.1074/jbc.M113.522375

Topham, C.H., and S.S. Taylor. 2013. Mitosis and apoptosis: How is the balance set? *Curr. Opin. Cell Biol.* 25:780–785. http://dx.doi.org/10.1016/j.ceb.2013.07.003

Trivedi, P., and P.T. Stukenberg. 2016. A centromere-signaling network underlies the coordination among mitotic events. *Trends Biochem. Sci.* 41:160–174. http://dx.doi.org/10.1016/j.tibs.2015.11.002

Tseng, B.S., L. Tan, T.M. Kapoor, and H. Funabiki. 2010. Dual detection of chromosomes and microtubules by the chromosomal passenger complex drives spindle assembly. *Dev. Cell.* 18:903–912. http://dx.doi.org/10.1016/j.devcel.2010.05.018

Tsukahara, T., Y. Tanno, and Y. Watanabe. 2010. Phosphorylation of the CPC by Cdk1 promotes chromosome bi-orientation. *Nature.* 467:719–723. http://dx.doi.org/10.1038/nature09390

Vader, G., J.J. Kauw, R.H. Medema, and S.M. Lens. 2006. Survivin mediates targeting of the chromosomal passenger complex to the centromere and midbody. *EMBO Rep.* 7:85–92. http://dx.doi.org/10.1038/sj.embor.7400562

Vader, G., C.W. Cruijsen, T. van Harn, M.J. Vromans, R.H. Medema, and S.M. Lens. 2007. The chromosomal passenger complex controls spindle checkpoint function independent from its role in correcting microtubule kinetochore interactions. *Mol. Biol. Cell.* 18:4553–4564. http://dx.doi.org/10.1091/mbc.E07-04-0328

van der Horst, A., M.J. Vromans, K. Bouwman, M.S. van der Waal, M.A. Hadders, and S.M. Lens. 2015. Inter-domain cooperation in INCENP promotes Aurora B relocation from centromeres to microtubules. *Cell Reports.* 12:380–387. http://dx.doi.org/10.1016/j.celrep.2015.06.038

van der Waal, M.S., A.T. Saurin, M.J. Vromans, M. Vleugel, C. Wurzenberger, D.W. Gerlich, R.H. Medema, G.J. Kops, and S.M. Lens. 2012. Mps1 promotes rapid centromere accumulation of Aurora B. *EMBO Rep.* 13:847–854. http://dx.doi.org/10.1038/embor.2012.93

Vigneron, S., S. Prieto, C. Bernis, J.C. Labbé, A. Castro, and T. Lorca. 2004. Kinetochore localization of spindle checkpoint proteins: Who controls whom? *Mol. Biol. Cell.* 15:4584–4596. http://dx.doi.org/10.1091/mbc.E04-01-0051

Vleugel, M., M. Omerzu, V. Groenewold, M.A. Hadders, S.M. Lens, and G.J. Kops. 2015. Sequential multisite phospho-regulation of KNL1-BUB3 interfaces at mitotic kinetochores. *Mol. Cell.* 57:824–835. http://dx.doi.org/10.1016/j.molcel.2014.12.036

Wang, E., E.R. Ballister, and M.A. Lampson. 2011. Aurora B dynamics at centromeres create a diffusion-based phosphorylation gradient. *J. Cell Biol.* 194:539–549. http://dx.doi.org/10.1083/jcb.201103044

Wang, F., J. Dai, J.R. Daum, E. Niedzialkowska, B. Banerjee, P.T. Stukenberg, G.J. Gorbsky, and J.M. Higgins. 2010. Histone H3 Thr-3 phosphorylation by Haspin positions Aurora B at centromeres in mitosis. *Science.* 330:231–235. http://dx.doi.org/10.1126/science.1189435

Welburn, J.P.I., M. Vleugel, D. Liu, J.R. Yates III, M.A. Lampson, T. Fukagawa, and I.M. Cheeseman. 2010. Aurora B phosphorylates spatially distinct targets to differentially regulate the kinetochore-microtubule interface. *Mol. Cell.* 38:383–392. http://dx.doi.org/10.1016/j.molcel.2010.02.034

Xu, P., E.A. Raetz, M. Kitagawa, D.M. Virshup, and S.H. Lee. 2013. BUBR1 recruits PP2A via the B56 family of targeting subunits to promote chromosome congression. *Biol. Open.* 2:479–486. http://dx.doi.org/10.1242/bio.20134051

Xue, J.Z., E.M. Woo, L. Postow, B.T. Chait, and H. Funabiki. 2013. Chromatin-bound *Xenopus* Dppa2 shapes the nucleus by locally inhibiting

microtubule assembly. *Dev. Cell.* 27:47–59. http://dx.doi.org/10.1016/j.devcel.2013.08.002

Yamagishi, Y., T. Honda, Y. Tanno, and Y. Watanabe. 2010. Two histone marks establish the inner centromere and chromosome bi-orientation. *Science.* 330:239–243. http://dx.doi.org/10.1126/science.1194498

Yamagishi, Y., C.H. Yang, Y. Tanno, and Y. Watanabe. 2012. MPS1/Mph1 phosphorylates the kinetochore protein KNL1/Spc7 to recruit SAC components. *Nat. Cell Biol.* 14:746–752. http://dx.doi.org/10.1038/ncb2515

Yang, Y., F. Wu, T. Ward, F. Yan, Q. Wu, Z. Wang, T. McGlothen, W. Peng, T. You, M. Sun, et al. 2008. Phosphorylation of HsMis13 by Aurora B kinase is essential for assembly of functional kinetochore. *J. Biol. Chem.* 283:26726–26736. http://dx.doi.org/10.1074/jbc.M804207200

Yang, Z., A.E. Kenny, D.A. Brito, and C.L. Rieder. 2009. Cells satisfy the mitotic checkpoint in Taxol, and do so faster in concentrations that stabilize syntelic attachments. *J. Cell Biol.* 186:675–684. http://dx.doi.org/10.1083/jcb.200906150

Zeitlin, S.G., R.D. Shelby, and K.F. Sullivan. 2001. CENP-A is phosphorylated by Aurora B kinase and plays an unexpected role in completion of cytokinesis. *J. Cell Biol.* 155:1147–1157. http://dx.doi.org/10.1083/jcb.200108125

Zhu, T., Z. Dou, B. Qin, C. Jin, X. Wang, L. Xu, Z. Wang, L. Zhu, F. Liu, X. Gao, et al. 2013. Phosphorylation of microtubule-binding protein Hec1 by mitotic kinase Aurora B specifies spindle checkpoint kinase Mps1 signaling at the kinetochore. *J. Biol. Chem.* 288:36149–36159. http://dx.doi.org/10.1074/jbc.M113.507970

Zich, J., A.M. Sochaj, H.M. Syred, L. Milne, A.G. Cook, H. Ohkura, J. Rappsilber, and K.G. Hardwick. 2012. Kinase activity of fission yeast Mph1 is required for Mad2 and Mad3 to stably bind the anaphase promoting complex. *Curr. Biol.* 22:296–301. http://dx.doi.org/10.1016/j.cub.2011.12.049

Zierhut, C., C. Jenness, H. Kimura, and H. Funabiki. 2014. Nucleosomal regulation of chromatin composition and nuclear assembly revealed by histone depletion. *Nat. Struct. Mol. Biol.* 21:617–625. http://dx.doi.org/10.1038/nsmb.2845